Structural Validation, Restoration, and Prediction

11.1 Introduction

This chapter presents techniques for validating structural interpretations and for extracting additional information, such as the shape of the structure beyond the data, predicting the presence of structures too small to be seen at the resolution of the data, and determining the structural evolution. Most of the techniques of structural restoration, balance and prediction are related to one another by use of a common set of kinematic models, which is why they will be discussed together here.

A restorable structure can be returned to its original, pre-deformation geometry with a perfect or near-perfect fit of all the segments in their correct pre-deformation order (Fig. 11.1). Restoration is a fundamental test of the validity of the interpretation. A restorable structure is internally consistent and therefore has a topologically possible geometry. An unrestorable structure is topologically impossible and therefore is geologically not possible (Dahlstrom 1969). An interpretation based on a large amount of hard data, such as a complete exposure, many wells, or good seismic depth sections controlled by wells, is nearly always restorable, whereas interpretations based on sparse data are rarely restorable. This is the empirical evidence that validates restoration as a validation technique.

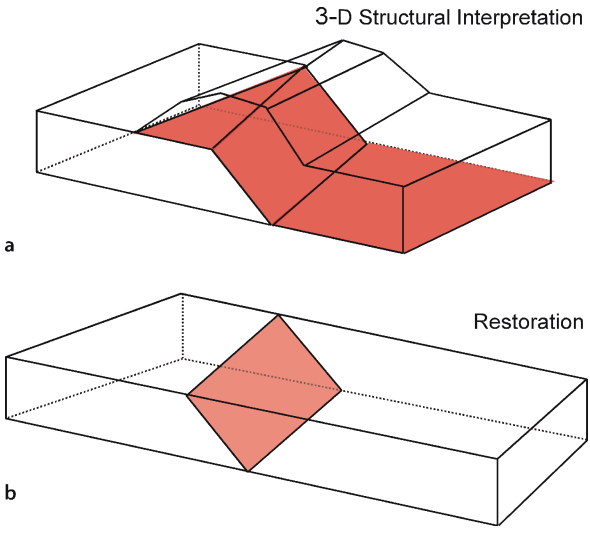

Fig. 11.1. A three-dimensional structural interpretation (**a**) and its restoration (**b**). The *shaded surface* is a fault

The original concept of a balanced cross section (Chamberlin 1910) is that the deformed-state and restored cross sections maintain constant area and so would balance on a beam balance (Fig. 11.2). This concept was generalized by Dahlstrom (1969) to a constant volume criterion. In many structures there is little or no deformation along the axis of the structure, and so in practice the third dimension can often be temporarily ignored and constancy of volume can be applied to a cross section as a constant-area rule. Units which maintain constant bed length are said to be length balanced and units that maintain constant area but not constant bed length or bed thickness are said to be area balanced. A balanced cross section is generally understood to be one which is restorable to a geologically reasonable pre-deformation geometry, as well as maintaining constant area.

The techniques for the restoration of a structure are necessarily based on models for the evolution of the geometry. A kinematic model defines the evolution through time of the geometry of a structure. Four basic kinematic models are commonly used for restoration (Fig. 11.3). The most appropriate model for a given structure will be determined by the mechanical stratigraphy and the boundary conditions that produced the structure. The simplest model is rigid-body displacement (Fig. 11.3a) which may include both translation and rotation. Layer-parallel slip (Fig. 11.3b) implies slip between closely spaced layers that maintain constant thickness unless otherwise specified. If the slip is between layers that are visible at the scale of observation, the folding mechanism is known as flexural slip (Donath and Parker 1964) and so this is called the

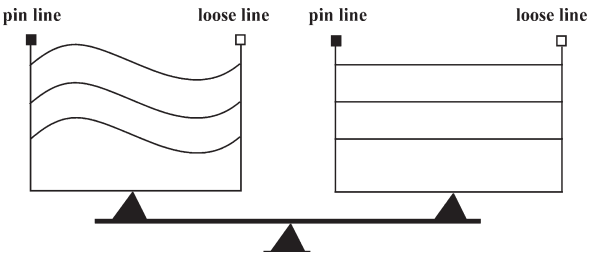

Fig. 11.2.
The concept of a balanced cross section (after Woodward in Woodward et al. 1989). Deformed-state section on the left, restored section on the right

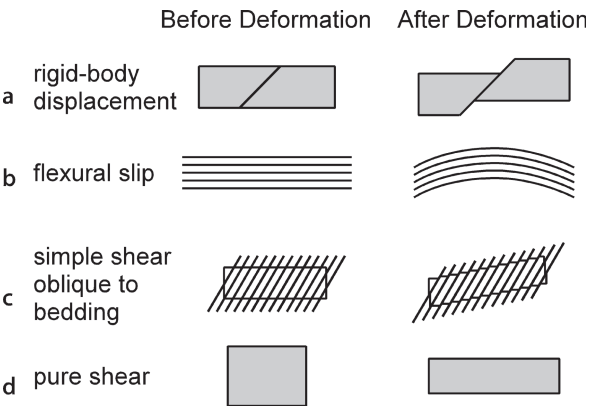

Fig. 11.3.
Basic kinematic models. **a** Rigid-body displacement. **b** Flexural slip. **c** Simple shear oblique to bedding. **d** Pure shear

flexural-slip model. Simple shear is the geometry produced by slip on closely spaced, parallel planes with no length or thickness changes parallel or perpendicular to the slip planes. Simple shear parallel to bedding is the mechanism of flexural slip. Simple shear oblique to bedding (Fig. 11.3c) is a kinematic model that causes bed length and bed thickness changes. Pure shear is an area-constant shape change (Fig. 11.3d) for which the shortening in one direction is exactly balanced by extension at right angles to it. Restorations are produced by applying one or more of these kinematic models to the deformed-state structure to return it to its pre-deformation configuration.

A valid map or cross section may be restorable by more than one kinematic model, and different models will produce somewhat different restored geometries. It follows that any given restoration does not necessarily represent the exact pre-deformation geometry or the specific path followed by the structural evolution. Nevertheless, the internal consistency of the restoration by any technique constitutes a validation of the interpretation. If a restoration is possible, it shows that the structure is internally consistent even if the restoration technique is not a perfect model for the deformation process.

Kinematic models contain the relationships needed to predict the geometry and evolution of a structure. The predictive capabilities of the models are the basis of techniques for utilizing very limited amounts of information to predict the geometry in areas of very sparse data or no data (Fig. 11.4). This chapter introduces the basic kinematic models and their predictive capabilities.

Kinematic models represent simplified descriptions of the mechanical processes that form structures. The deformation in some structures is more complex than can be fit by one of the simple kinematic models. For these structures the more general area-balancing methods can be appropriate. Using the relationship between displaced area and depth, a structure can be tested for area balance and its lower detachment predicted without performing a restoration or a model-based prediction. Layer-parallel strain is treated here because it is an intrinsic part of both the kinematic models and the area-depth relationship and because it provides a tool for predicting sub-resolution structure (i.e., folds and faults too small to be seen at the resolution of the data) and is another tool for validating the structural interpretation.

The chapter begins with the most general concepts, an overview of balance and restoration followed by a discussion of strain and strain partitioning. Then the model-independent area-balance methods and area-depth technique are given, followed by the individual kinematic-model-based restoration and prediction techniques.

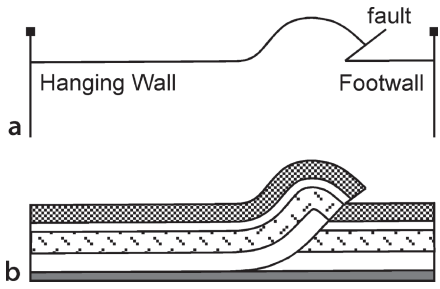

Fig. 11.4.
Prediction of fault shape from geometry of a key bed using the flexural-slip kinematic model (after Geiser et al. 1988). **a** Key bed required for prediction. **b** Predicted complete hangingwall geometry and fault shape

11.2 Restoration and Balance

This section covers general concepts and terminology used in all the balancing and restoration techniques to follow.

11.2.1 Boundaries

Ideally, the boundaries of a section to be restored are chosen so that the section will restore to a rectangle (Fig. 11.5a). The side boundaries are pin lines, and the upper boundary is a reference bed that will be returned to its original depositional geometry (Dahlstrom 1969; Elliott in Geiser 1988; Marshak and Woodward 1988). The original position of a horizon, including both its shape and elevation, is known as the *regional datum*, commonly shortened to just the *regional* (McClay 1992). The restored positions of all other horizons are determined with respect to the reference horizon. The base of the section is normally either a stratigraphic marker or a detachment horizon (Fig. 11.5), but may be simply the lowest visible unit. The bounding pin lines are leading and trailing pins, according to their position in the structure with respect to the transport direction. A locally balanced structure is one in which bed-normal pins on either side of the structure of interest define a region in which the area has remained

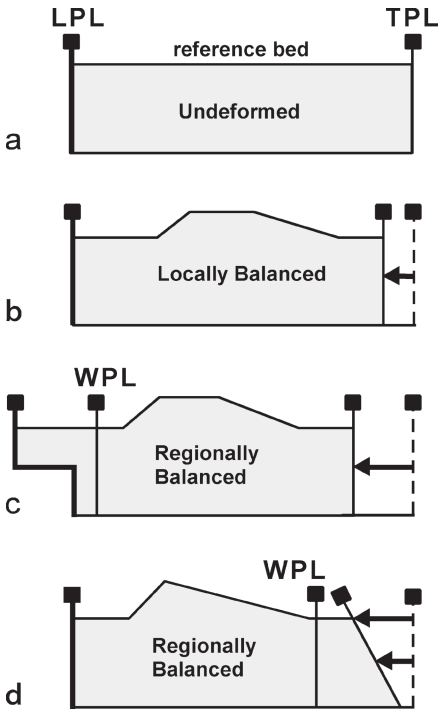

Fig. 11.5. Pin lines bounding a region of interest. *LPL:* leading pin line; *TPL:* trailing pin line; *WPL:* working pin line. **a** Undeformed. **b** Locally balanced. **c** Regionally balanced with transport of material out of the structure. **d** Regionally balanced with simple-shear transport of material into the structure

constant (Fig. 11.5b). If material has been transported across the chosen pin lines by displacement on an upper detachment (Fig. 11.5c) or into or out of the region by layer-parallel simple shear (Fig. 11.5d), the structure should be regionally balanced, even if the region of interest is not locally balanced. Thus for a regionally balanced structure a vertical pin lines may represent a *working* pin line (Fig. 11.5b,c) that will restore with an offset or a tilt. A valid cross section might fail to restore to a rectangle because of unrecognized transport across a working pin line. The restoration reveals these otherwise hidden displacements.

11.2.2 Palinspastic vs. Geometric Restoration

Restoration is a purely geometric manipulation of the cross section according to a specific set of rules. A geometric restoration (Fig. 11.6) is a restoration that is not specifically related to the direction of transport that formed the structure. A palinspastic restoration is the restoration of the units to their correct pre-deformation configuration by exactly reversing the displacements that formed the structure. The independence of the restoration from the transport direction is illustrated in Fig. 11.6. Two different cross sections through a fold have been restored. Normally it is assumed that

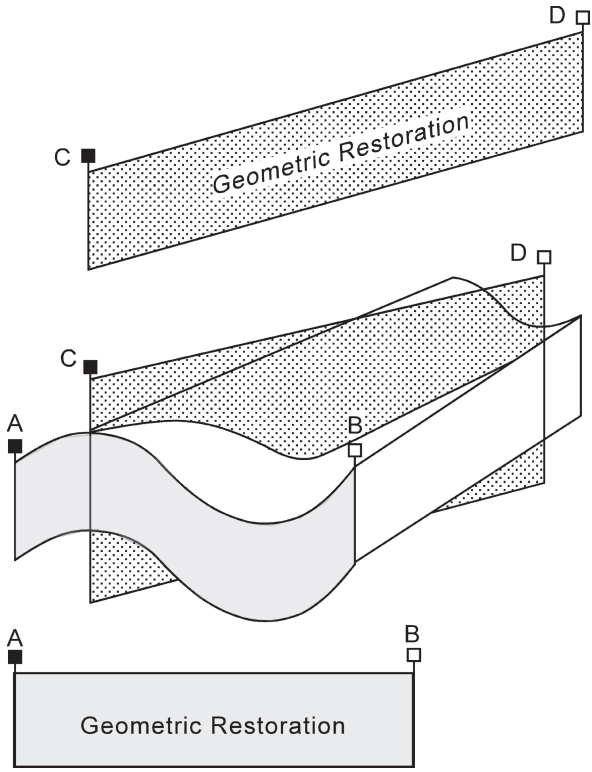

Fig. 11.6.
Geometric restoration of a cross section in any direction

the transport direction is perpendicular to the fold axis, and so the palinspastically restored section would be AB. If the transport is in the CD direction, however, the palinspastic restoration would be in the CD cross section. Either restoration serves to validate the structure but only the palinspastic restoration returns the units to their actual pre-deformation locations.

The only restriction on the choice of the orientation of the line of section is that the transport direction should be approximately constant in the vicinity of the cross section (Elliott 1983; Woodcock and Fischer 1986). The transport direction need not be parallel to the line of section as long as faults with transport oblique to the section are not crossed. A cross section oblique to the transport direction is the same as a section having vertical or horizontal exaggeration (Cooper 1983, 1984; Washington and Washington 1984). This exaggeration can be removed by projecting the section into the transport direction (Sects. 6.5, 6.6). Restoration of a cross section that crosses oblique-transport faults will probably result in a structural or stratigraphic discontinuity at the fault. The discontinuity might be removed by a lateral shift of the cross section at the fault.

As an example of the difference between geometric and palinspastic restoration, consider restoring the Säntis anticline, a major fold above the Säntis thrust in the Helvetic fold and thrust belt of Switzerland (Fig. 11.7). The anticline is oblique to the

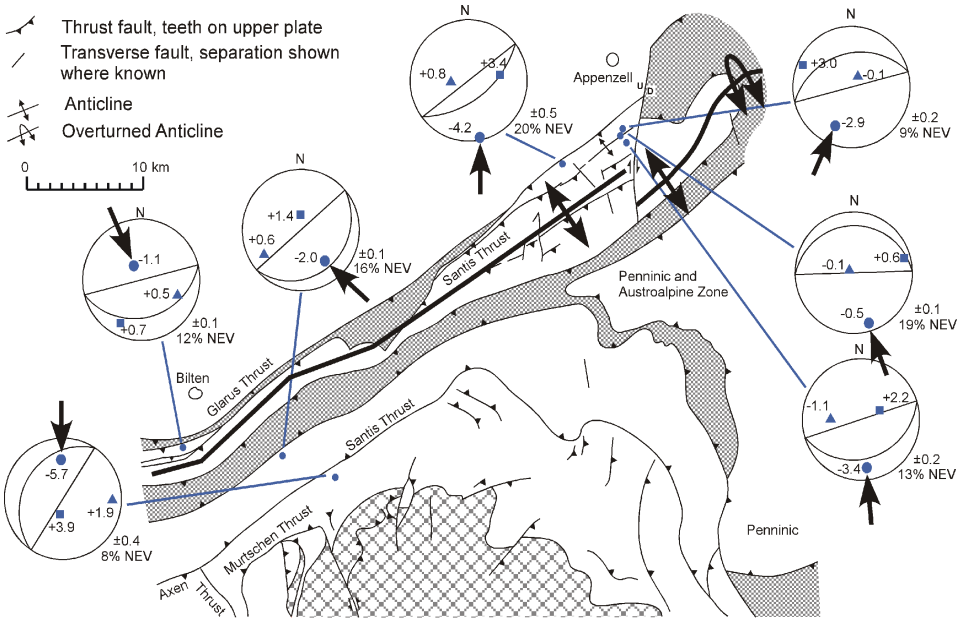

Fig. 11.7. Geologic map of the Säntis anticline in the Helvetic fold-thrust belt, eastern Switzerland constructed at a 1 500 m datum (modified from Groshong et al. 1984). Calcite twin-strain axes are shown on lower-hemisphere, equal-area stereograms: *dot:* maximum shortening axis; *square:* maximum extension axis; *triangle:* intermediate strain axis. *Large arrows* show transport direction interpreted as being parallel to the direction of internal shortening strain

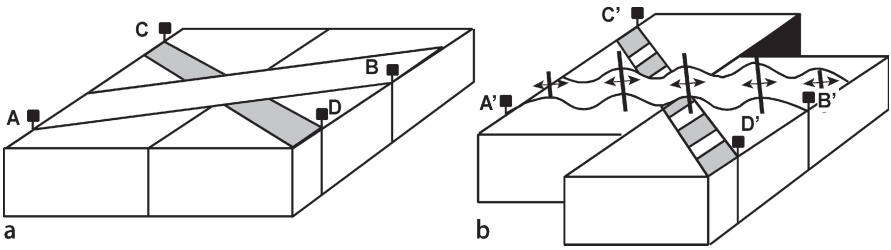

Fig. 11.8. Deformation in beds above a strike-slip fault. **a** Before deformation. **b** After right-lateral strike-slip displacement. Both cross sections A'B' and C'D' can be geometrically restored without removing the rotation caused by the strike-slip displacement

regional northward transport direction documented by the north-south pebble elongation direction observed in exposures of the basal thrust and the mainly north-south twinned-calcite shortening strains in the fold itself (Fig. 11.7). The fold axis orientation may be controlled by an underlying oblique thrust ramp. A palinspastic restoration of this anticline requires a north-south cross section. The section perpendicular to the fold axis can be restored, but it would be a geometric, not a palinspastic, restoration.

The distinction between a palinspastic and geometric restoration is important to the use of balancing techniques along wrench faults. Figure 11.8 shows representative portions of beds deformed by movement along a wrench fault. Strike-slip displacement on the fault produces shortening and rotation of section AB to the final position A'B'. Deformation dies out away from the master fault and so the pin lines at A' and B' are both in undeformed beds. The cross section A'B' could be restored, as could any other line of section. A correct palinspastic restoration requires the vertical-axis rotation to be restored as well. The line CD (Fig. 11.8) will be extended and rotated during wrench deformation into the position C'D'. Extensional structures such as normal faults will develop perpendicular to this line and could also be geometrically restored. Restorations across small-displacement wrench faults can be expected to be relatively free from major discontinuities. Restorations across large-displacement wrench faults are likely to show large discontinuities at the master fault but otherwise be restorable.

11.2.3 Sequential Restoration

A sequential restoration shows the intermediate stages between the fully deformed and fully restored stages. Where growth stratigraphy is present, the geometry of the intermediate stages is controlled by the thickness changes (Fig. 11.9). A sequential restoration is valuable because of the insight it provides into the structural evolution and because it represents an even more rigorous test of the validity of the interpretation. A sequential restoration of a section consisting entirely of pre-growth units is possible, but must be based on the kinematic model, rather than on hard data.

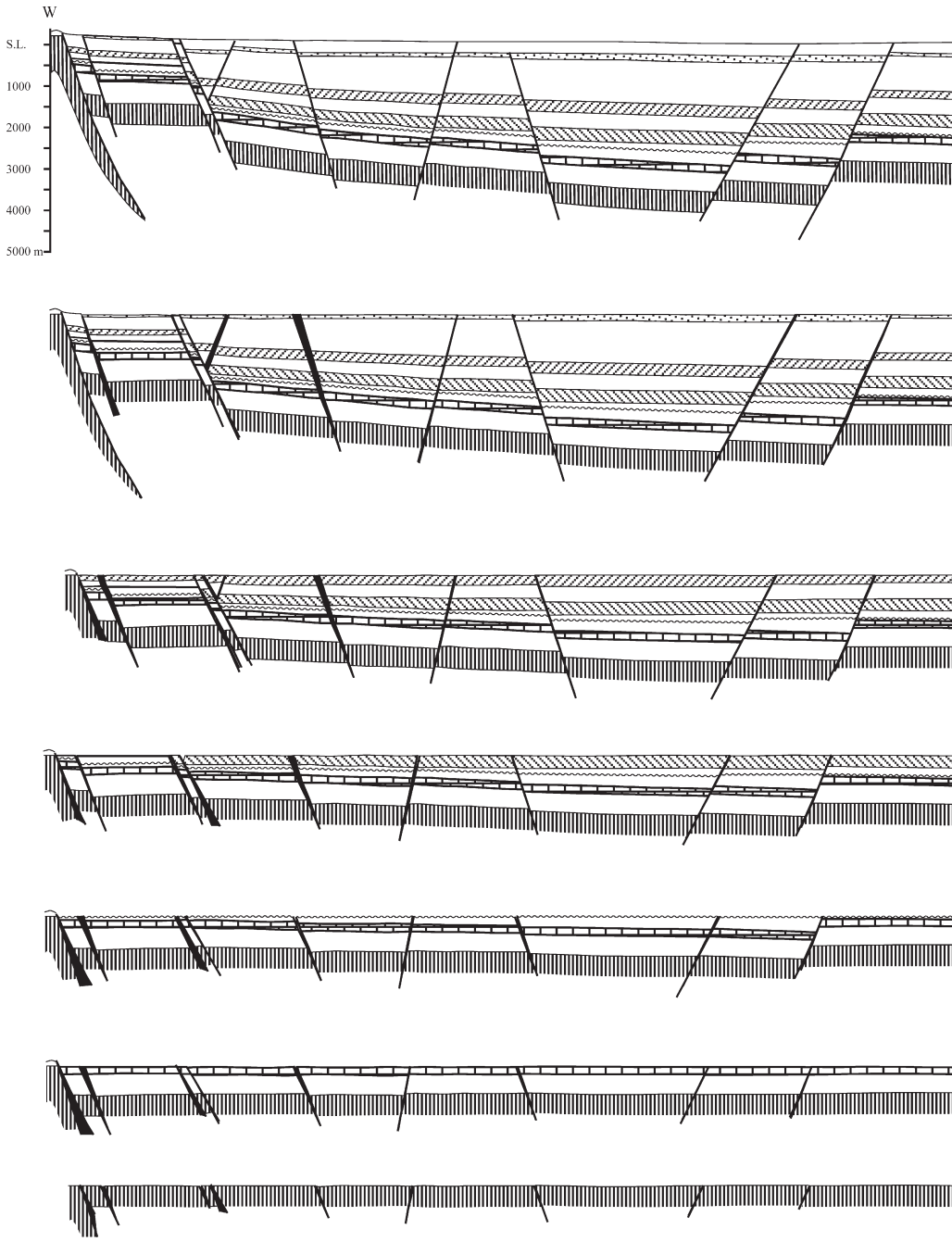

Fig. 11.9. Sequential restoration of a profile across the Rhine Graben, Germany. The upper cross section is redrawn from Doebl and Teichmüller (1979). Gaps between blocks are *black*

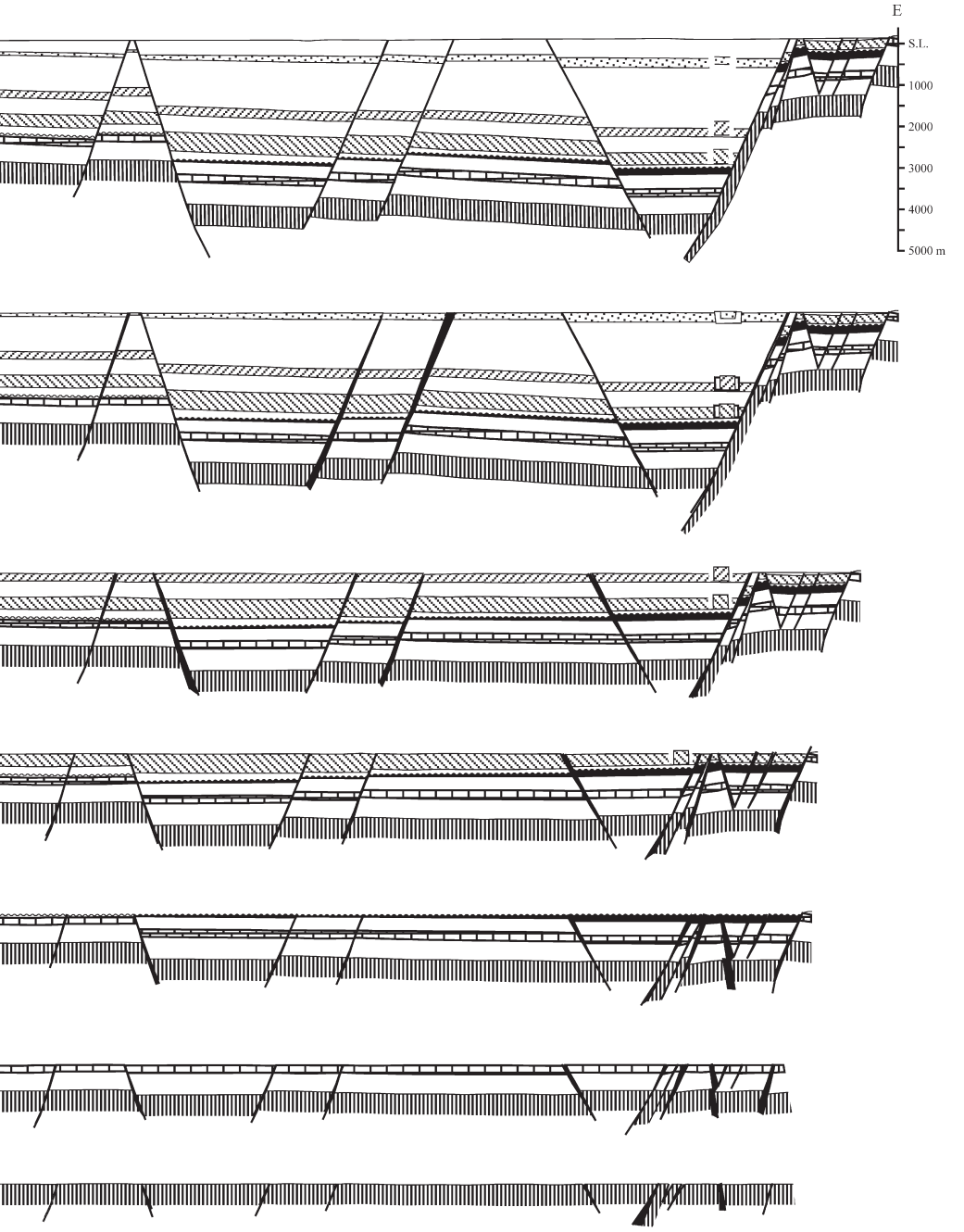
E
S.L.
1000
2000
3000
4000
5000 m

11.3 Strain and Strain Partitioning

Strain can play a significant role in structural balancing. Presented here are the practical strain measurements that can be applied to field examples at the map and cross-section scale. The most readily quantifiable macroscopic measures of strain are bed length and bed thickness (Fig. 11.10). Separate equations are given for the strain parallel and perpendicular to bedding, even though the forms are identical, in order to better emphasize the origins of the interpretations that will appear in subsequent sections.

Bed length change can be quantified as

$$\Delta L = L_1 - L_0 \quad , \tag{11.1}$$

$$e_L = (L_1 - L_0) / L_0 \quad , \text{or} \tag{11.2}$$

$$e_L = (L_1 / L_0) - 1 \quad , \tag{11.3}$$

where ΔL = change in bed length, e_L = the infinitesimal normal strain parallel to bedding, L_0 = the bed length before deformation, L_1 = the bed length after deformation. Exactly equivalent equations can be written for bed thickness change:

$$\Delta t = t_1 - t_0 \quad , \tag{11.4}$$

$$e_t = (t_1 - t_0) / t_0 \quad , \text{or} \tag{11.5}$$

$$e_t = (t_1 / t_0) - 1 \quad , \tag{11.6}$$

where Δt = change in bed thickness, e_t = the infinitesimal normal strain perpendicular to bedding, t_0 = the bed thickness before deformation, t_1 = the bed thickness after deformation. With the equations in the forms given, extension is positive and contraction is negative. The value of e is a fraction but is commonly given as a percent by multiplying by 100.

The strain can be also be measured with the stretch, β, (McKenzie 1978):

$$\beta_L = (L_1 / L_0) \quad , \tag{11.7}$$

$$\beta_t = (t_1 / t_0) \quad , \tag{11.8}$$

where β_L = layer-parallel stretch and β_t = layer-normal stretch. The stretch is always positive, greater than 1 for extension and less than 1 for contraction. For a constant area rectangle the stretch has the convenient property that

$$\beta_L = 1 / \beta_t \quad . \tag{11.9}$$

From Eqs. 11.7, 11.8 and 11.9, the stretches can also be given as

$$\beta_L = t_0 / t_1 \quad , \tag{11.10}$$

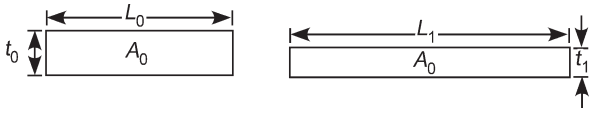

Fig. 11.10.
Bed length and bed thickness change in an area-constant deformation

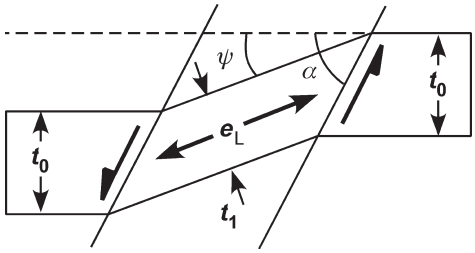

Fig. 11.11.
Deformation of a bed of original thickness t_0 by oblique simple shear (after Groshong 1990). α: angle between shear direction and bedding, ψ: angle of shear, e_L: layer-parallel extension

$$\beta_t = L_0 / L_1 \quad , \tag{11.11}$$

and from Eqs. 11.3, 11.6 and 11.7, 11.8,

$$e_L = \beta_L - 1 \quad , \tag{11.12}$$

$$e_t = \beta_t - 1 \quad . \tag{11.13}$$

Simple shear oblique to bedding (Fig. 11.11) changes the bed length and bed thickness. The layer-parallel strain can be determined from the shear amount and the shear angle (Groshong 1990) as

$$e_L = [\sin \alpha / \sin (\alpha - \psi)] - 1 \quad , \text{ or} \tag{11.14}$$

$$e_{90} = (1 / \cos \psi) - 1 \quad , \tag{11.15}$$

where α = angle between shear direction and bedding and ψ = angle of shear. Equation 11.15 is for vertical simple shear ($\alpha = 90°$) and Eq. 11.14 is for all other angles. To find the thickness change from the length change for constant area deformation, substitute Eq. 11.3 into 11.6 to give

$$e_t = -e_L / (e_L + 1) \quad . \tag{11.16}$$

Simple shear parallel to bedding in flexural-slip deformation has no effect on bed length or bed thickness. If a bed-normal marker is present, or assumed, then its length strain is given by Eq. 10.15 where the angle of shear is the amount of rotation of the original bed-normal marker.

Strain is commonly partitioned between deformation features that are visible at the scale of the map and cross section and deformation at smaller scales, termed sub-resolution strain. In the low-temperature deformation of lithified rocks (i.e., where hydrocarbons can be preserved), the crystal-plastic strains are usually less than

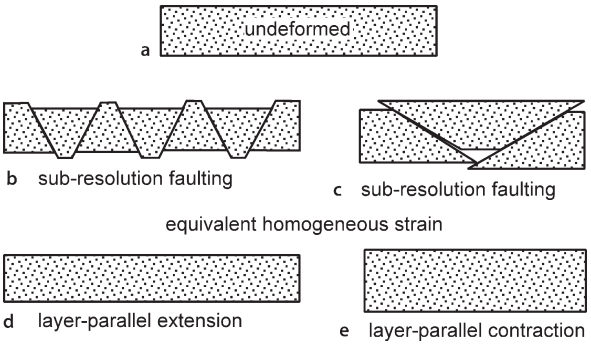

Fig. 11.12.
Representative segment of a bed deformed by sub-resolution strain. **a** Undeformed. **b** Extension on small normal faults. **c** Contraction on small thrust faults. **d** Low-resolution observation of **b**. **e** Low-resolution observation of **c**

4–6%, and perhaps closer to 1–2% in very brittle lithologies such as dolomite or in extensional settings (Groshong 1988). If the deformation is brittle, additional strain within the layers will commonly be accommodated by small-scale faulting (Fig. 11.12b,c). Strain measured at the scale of the oil field or a seismic line may appear homogeneous (Fig. 11.12d,e) but represent the combined effects of sub-resolution faults and/or folds.

11.4 Area-Balance Methods

Area balance methods include the restoration of irregularly shaped deformed regions, area-based depth-to-detachment calculations and the area-depth relationship. These methods do not depend on specific kinematic models and in that sense represent the most general approaches to validation, restoration, and prediction. All the structures discussed in Sects. 11.4.1–11.4.3 are locally balanced (Fig. 11.5b). Regionally balanced structures (Fig. 11.5c,d) will be treated in Sect. 11.4.4.

11.4.1 Area Restoration

Area restoration is used for structures in which deformation has produced significant changes in the original bed lengths and thicknesses. The technique is based on the area of the deformed-state cross section (Fig. 11.13a). It is assumed that the area has remained constant:

$$A_0 = t_0 \, L_0 \quad , \tag{11.17}$$

where A_0 = original area, t_0 = original bed thickness, and L_0 = original bed length. The area between the pin lines is measured and then divided by either the original bed thickness or the original bed length, whichever is better known, and Eq. 11.17 solved for the unknown dimension. The original bed length might be known from that of an adjacent key bed that has not changed thickness (Mitra and Namson 1989) or the original thickness might be known from a location outside the deformed region. The shape

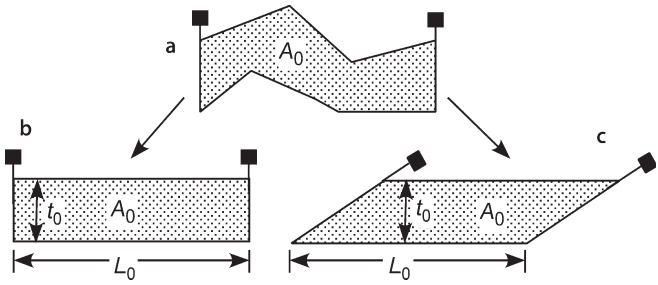

Fig. 11.13.
Area restoration. A_0: Original area; t_0: original bed thickness; L_0: original bed length. Shape of the restored area depends on assumed original orientations of the pin lines. **a** Deformed-state cross section. **b** Section restored to vertical pin lines. **c** Section restored to tilted pin lines

of the restored area depends on the assumed original shape (Mitra and Namson 1989). Ordinarily the unit is restored to horizontal, leaving only the orientations of the pin lines to be determined. A folded area might be appropriately restored to a rectangular prism (Fig. 11.13b), whereas a block bounded by faults would be restored to fit between the presumed original fault shapes (Fig. 11.13c).

11.4.2
Depth to Detachment and Layer-Parallel Strain

The first predictive uses of the concept of area balance were to determine the depth to detachment of the structure (Chamberlin 1910; Hansen 1965). Area uplifted above the regional as a result of compressional deformation is termed the excess area (Fig. 11.14). Area that drops below regional as a result of extensional deformation is termed lost area. More generally, these can be called the displaced areas. The classical displaced-area method is designed to find the detachment depth from the excess or lost area of one horizon in a structure. The displaced area is produced by displacement along the lower detachment such that

$$S = D\,H \quad , \tag{11.18}$$

where S = area above or below the regional, D = displacement, and H = depth to detachment from regional (Fig. 11.14). A unique depth to detachment can be calculated from a measurement of the excess area *if* the displacement that formed the structure is known. Chamberlin (1910) and many subsequent authors have assumed that bed length remains constant and so the displacement is the difference between the curved-bed length of the marker horizon and its length at regional:

$$D = L_0 - W \quad , \tag{11.19}$$

where D = displacement, L_0 = curved-bed length (assumed equal to original bed length) and W = width of structure at regional. Substituting Eq. 11.19 into 11.18:

$$H_c = S / (L_0 - W) \quad , \tag{11.20}$$

where H_c indicates the detachment depth if bed length is constant.

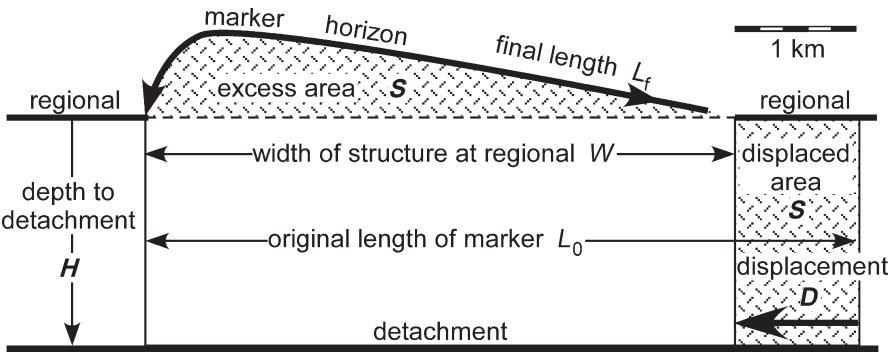

Fig. 11.14. Area balanced model. $H = 2.08$ km, $L_f = 5.422$ km, $S = 2.141$ km^2, $W = 4.879$ km, $D = 1.028$ km. Theoretical detachment for constant bed length is $H = 3.943$ km (Eq. 11.20)

Fig. 11.15. Detachment depth vs. strain diagram, for the model in Fig. 11.14, shortening negative

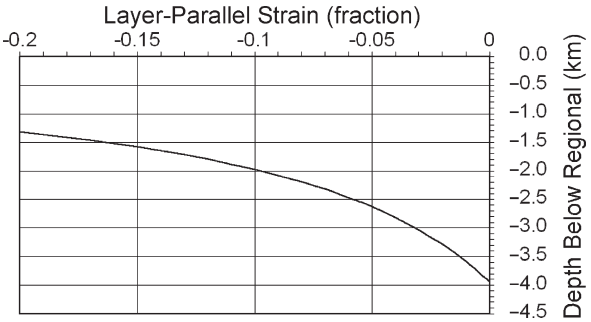

Calculations based on constant bed length typically show detachments that are extremely deep for low-amplitude structures and indicate shallower detachments for higher-amplitude structures, even in the same area (eg., the Appalachian profile of Chamberlin 1910). One significant problem is the assumption of constant bed length. Previous work (Groshong 1988, 1994) has shown that bed length is not likely to remain constant and that length changes can have a significant effect on the calculated detachment depth. For example, the theoretical depth to detachment of the area-balanced model in Fig. 11.14 is 3.943 km (Eq. 11.20), about 90% greater than the correct value of 2.08 km. The sensitivity of the calculated detachment depth to unmeasured changes in bed length (sub-resolution strain) can be demonstrated quantitatively. If the bed length changes during deformation,

$$L_f = L_0 + \Delta L \quad , \tag{11.21}$$

where L_f = observed length = final bed length (Fig. 11.14) and ΔL = change in bed length during deformation (shortening negative). Equation 11.21 is solved for L_0 and substituted into Eq. 11.19, giving the relationship between D and the changing bed length. This relationship is substituted into Eq. 11.18 and solved for H to give

$$H = S / (L_f - \Delta L - W) \quad . \tag{11.22}$$

If $\Delta L = 0$, then $L_f = L_0$, and this equation reduces to the constant bed-length relationship (Eq. 11.20).

The effect of bed-length change on the depth-to-detachment relationship for the example in Fig. 11.14 is seen by substituting the measured values of S, L_f, W, and a range of ΔL values (including zero) into Eq. 11.22 and graphing the result (Fig. 11.15). The most general result is obtained by plotting layer-parallel strain (Eq. 11.2) versus detachment depth. The maximum possible detachment depth (3.943 km) occurs for zero strain. The detachment at 2.0 km shown in Fig. 11.14 requires a layer-parallel shortening of –0.1 (–10%) in the marker horizon. A shallower detachment is possible if the layer-parallel strain is sufficient.

11.4.3
Area-Depth Relationship of Locally Balanced Structures

The relationship between the areas of multiple horizons on a cross section and their depths allows a cross section to be tested for area balance and internal consistency without restoration. Detachment depth can be determined without knowledge of the layer-parallel strain, and the layer-parallel strain can be determined once the detachment location is known.

Displacement causes an amount of the original area to be pushed above the regional (excess area) or dropped below the regional (lost area) as shown in Fig. 11.16. Measurements are made of the excess or lost areas above or below the regional and the elevation of the regional with respect to the reference level for each horizon. This information is plotted on a graph of area versus depth (elevation) (Fig. 11.17a). For a locally balanced structure, the data from multiple horizons give points that define a straight line, the equation of which is

$$h = (1 / D)\ S + H_e \quad , \tag{11.23}$$

where h = elevation of a surface above or below the reference level, D = displacement on the lower detachment, S = net displaced area, either excess or lost, and H_e = the elevation at which the area S goes to zero, which represents the position of the detach-

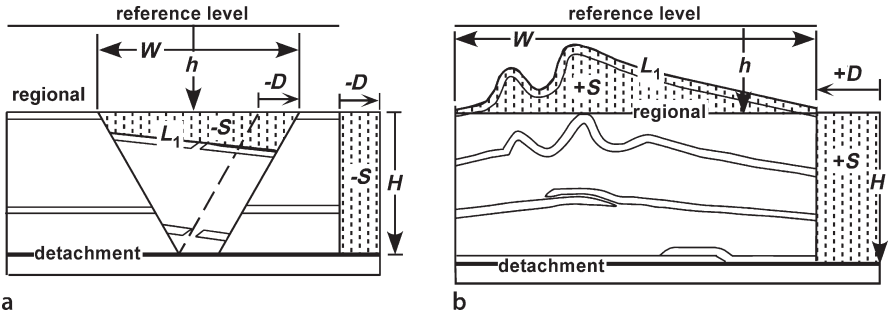

Fig. 11.16. Area-balance terminology. *S:* Excess or lost area; *D:* displacement on the lower detachment; *H:* distance from the lower detachment to the regional; *h:* elevation of the regional above or below the reference level; L_1: bed length after deformation. **a** Extension (after Groshong 1996). **b** Contraction (after Groshong and Epard 1994)

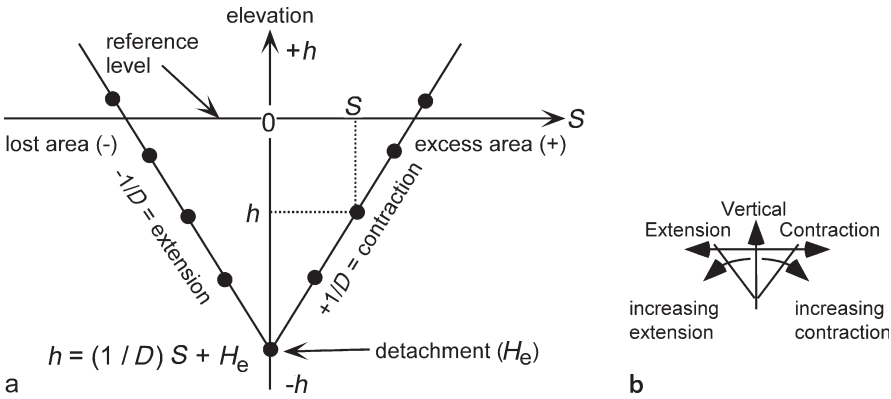

Fig. 11.17. Area-depth relationships for compressional and extensional detachment structures. **a** Area-depth graph. **b** Relationship between the slope of the area-depth line and the amount and type of deformation

ment. The elevation of the reference level is arbitrary. If the reference level is at the detachment, $H_e = 0$. If the reference level is chosen to be sea level, then H_e will be the elevation of the detachment relative to sea level. The sign convention for area is that excess area and contractional displacement are positive and lost area and extensional displacement are negative. If deformation causes both uplift and subsidence from the regional, the correct value of S is the algebraic sum or net area (Groshong 1994). The slope of the area-depth line, $1 / D$, is the inverse of the displacement on the lower detachment. To be a valid cross section, the points on the area-depth graph (Fig. 11.17a) must all fall on or close to the area-depth line.

Each horizon has its own separate regional. The reference level should be at least approximately parallel to the directions of the regionals and the elevations measured perpendicular to it. If the regionals are tilted with respect to the reference level, the elevation measurements should be taken at the center of the structure (equivalent to the average value).

Equation 11.23 and the graph in Fig. 11.17a are modified from the forms originally given by Epard and Groshong (1993) in order to show elevation as the vertical axis on the graph. This makes the graphical relationship between area and depth more intuitively obvious, with the area on the area-elevation line decreasing downward on the graph to zero at the lower detachment (Fig. 11.17a), as it does in the structure itself (Fig. 11.16). In this form, a vertical area-depth line represents differential vertical displacement (Fig. 11.17b) and the lower the slope of the area-depth line, the greater the amount of extension or contraction. A positive slope of the line indicates contraction and a negative slope indicates extension. The slope of the area-depth line is the inverse of the displacement, instead of the displacement itself as in the previous formulation (Epard and Groshong 1993). For any given area-elevation data point, the range of h values caused by variations in measurement and interpretation will usually be significantly less than the range of the S values, and so a least-squares fit to the data should be a regression of S onto h, rather than h onto S as the form of Eq. 11.23 might suggest.

A potential pitfall with this technique is in the selection of the correct regional. The problem is that this level must be chosen on the deformed-state cross section. If undeformed units are preserved outside the structure of interest, they should record the correct elevation of the regional. The bottoms of synclines are good candidates for the elevations of the regionals in vertical and compressional structures and the elevations of beds in flat horsts are good candidates for the regionals in extensional structures. The effect of an incorrect choice of the regional is to produce an incorrect elevation for the lower detachment. The goodness of fit of the area-depth points to a line on the graph is unaffected by the choice of the regional, and so the method remains valuable in judging the internal consistency of the cross section, even if the regionals are unknown. Because the area-depth relationship is not dependent on the kinematic model, it applies as an additional constraint on model-based cross-section restorations and can provide additional information about the depth to detachment, strain and total displacement.

11.4.3.1 Effect of Growth Stratigraphy

The area-depth relationship described above applies to beds that were deposited before deformation. Displacement on the lower detachment of a locally balanced structure produces the same displacement in every pre-growth unit and results in a straight-line area-depth relationship. Growth beds are deposited during deformation and each bed may have a different displacement, the amount of which decreases upward in younger beds. Some of the lost area in the case of a graben (Fig. 11.18a) is filled with sediment. These effects result in an area-depth curve that is straight in the pre-growth units and curves upward toward zero area in the growth beds (Fig. 11.18b). The boundary between the growth and pre-growth intervals is clearly identified by the inflection point in the area-depth graph (horizon 6, Fig. 11.18b).

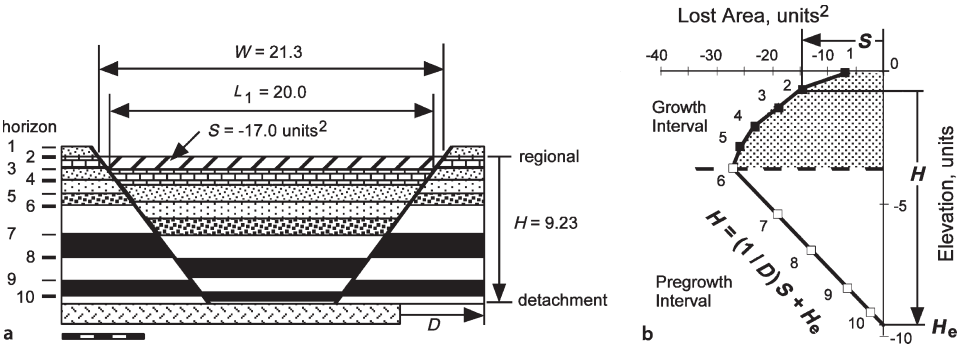

Fig. 11.18. Area-balanced model of a pure-shear full graben with growth sediments (Groshong et al. 2003a). **a** Cross section. *Solid black* and *solid white* layers are pre-growth units, *patterned* layers are growth beds. *Diagonal pattern* is the lost area of horizon 2. **b** Area-depth graph pointing out the values for horizon 2. *S:* lost area; *H:* depth to detachment for a particular horizon; *D:* displacement of pre-growth units; H_e*:* elevation of the lower detachment

11.4.3.2 Strain

Layer-parallel strain can be determined from the area-depth relationship if either the displacement is known (from the area-depth graph), or the detachment location is known (by direct observation or from the area-depth relationship). The method applies to growth beds as well as to pre-growth beds.

The length of a particular horizon as seen on a cross section is its final length L_1 which may include bed-length changes. From the geometry of Fig. 11.16, the original length of the horizon (L_0) is

$$L_0 = W + d = W + S/H \quad , \tag{11.24}$$

where W = the width of the structure at the regional of the horizon and d = the displacement of any horizon, including a growth horizon (Groshong et al. 2003a). A lowercase d is used here for a growth-bed displacement and an uppercase D for the total displacement of a pre-growth unit. Either value can be substituted into Eq. 11.24. W is always measured parallel to the regional and is tilted if the regional is tilted. The value of L_0 calculated from the displaced area is independent of the stratigraphic growth of the unit because it depends only on the length along the upper surface of the unit, not on the thickness. The bed-length change is

$$\Delta L = L_1 - L_0 = L_1 - (W + S/H) \quad . \tag{11.25}$$

The length difference can be converted to layer-parallel strain, e, by dividing Eq. 11.25 by Eq. 11.24:

$$e_L = (H\ L_1/(H\ W + S)) - 1 \quad . \tag{11.26}$$

If the total displacement, D, is known from the area-depth relationship, an alternative form of the equation is convenient:

$$e_L = (L_1/(W + D)) - 1 \quad . \tag{11.27}$$

11.4.4 Area-Depth Relationships of Regionally Balanced Structures

For regionally balanced structures, material is transported across vertical pin lines bounding the structure of interest (Fig. 11.5c,d). A representative example of a regionally balanced structure is a fault-bend fold (Figs. 11.5c, 11.19a). In a fault-bend fold, one of the original pin lines is offset along an upper detachment horizon (Fig. 11.19a). Part of the area displaced above the upper detachment is within the anticline and part is outside the anticline. Material may be displaced toward the foreland or toward the hinterland; the area-balance is the same. Two area-depth lines are produced, one for the stratigraphic levels below the upper detachment and one for the stratigraphic levels above the

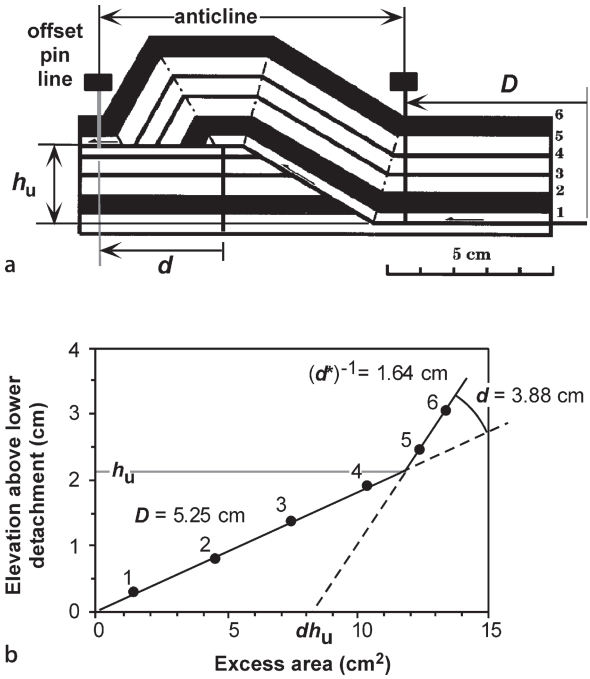

Fig. 11.19.
Area-depth relationships in a fold having displacement on an upper detachment. **a** Fault-bend fold model (after Suppe 1983). **b** Area-depth diagram of **a** (modified from Epard and Groshong 1993). *D:* displacement on lower detachment; *d*:* slope of line for horizons stratigraphically above the upper detachment; *d:* displacement on upper detachment; h_u*:* elevation of upper detachment

upper detachment. Below the upper detachment, no material is translated out of the section and the area-depth line is the same as for a locally balanced structure (Eq. 1.23). For units stratigraphically above the upper detachment, the area-depth line is

$$h_2 = [1 / (D - d)]\ S_2 + k \quad , \tag{11.28}$$

where h_2 = the distance from the reference level for units above the upper detachment, S_2 = the excess area of units stratigraphically above the upper detachment, d = displacement on the upper detachment, $k = d\, h_u / (D - d)$, and h_u = the elevation of the upper detachment. This is the equation of a line of slope $d^* = 1 / (D - d)$ that is valid for $h > h_u$. The excess areas of a fault-bend fold are thus distributed along two line segments (Fig. 11.19b). The lower-slope segment is valid for $h < h_u$ and corresponds to Eq. 11.23. The upper segment is valid for $h > h_u$ and corresponds to Eq. 11.28. The displacement on the upper detachment is the difference in the slopes of the two area-depth lines:

$$d = D - (d^*)^{-1} \quad . \tag{11.29}$$

Failure to recognize the presence of an upper detachment and taking into consideration only measurements from above the upper detachment will lead to a significant overestimation of the depth to detachment (lower dashed projection line on Fig. 11.19b). If the lower detachment is known to be shallower than the prediction, then an upper detachment is indicated.

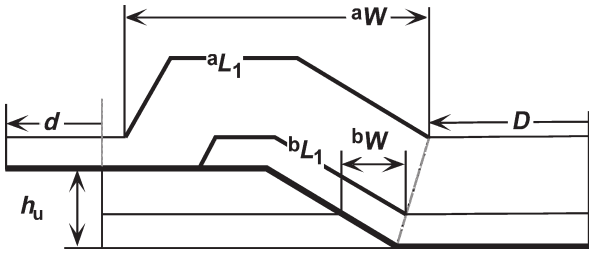

Fig. 11.20.
Length and displacement measurements for strain calculation

Sub-resolution strains are determined from the displacement and the width of the structure at regional. The appropriate relationship depends on whether the bed is stratigraphically below or above the level of the upper detachment horizon (Fig. 11.20). The final bed lengths are the observed lengths between the points where the structure departs from regional. The original bed lengths are given by the following equations:

$$^{b}L_0 = {}^{b}W + D \quad , \tag{11.30}$$

$$^{a}L_0 = {}^{a}W + (D - d) \quad , \tag{11.31}$$

where $^{i}L_0$ = original bed length, ^{i}W = width of structure parallel to regional at regional, i = a or b, D = displacement on the lower detachment, and d = displacement on the upper detachment. The layer-parallel strain is

$$e = (^{i}L_1 / {}^{i}L_0) - 1 \quad , \tag{11.32}$$

where e = layer-parallel strain as a fraction, $^{i}L_1$ = measured bed length, and $^{i}L_0$ = corresponding original bed length from Eqs. 11.30 or 11.31.

Other regionally balanced styles of importance are those produced with simple-shear transport of material into the closed structure (Fig. 11.5d). A linear shear profile has been treated by Epard and Groshong (1993). The total displacement is a combination of the constant component, D, and the distributed simple-shear component, D_s. The excess area is the sum of the constant-displacement component, Dh and the distributed shear component, S_s:

$$S = Dh + S_s \quad . \tag{11.33}$$

Assuming linear simple shear:

$$S_s = \tfrac{1}{2} D_s h \quad , \tag{11.34}$$

where

$$D_s = h \tan \psi \quad , \tag{11.35}$$

and ψ = angle of shear. Replacing D_s in Eq. 11.34 by 11.35 and substituting into Eq. 11.33 gives

$$h^2 \tfrac{1}{2}\tan\psi + h\ D - S = 0 \quad . \tag{11.36}$$

This is a quadratic equation in h of a curve through the origin.The curvature of the area-depth line is a constant that depends on the shear angle. If the shear angle is low, the value of tan ψ is small, the curvature is not very great, and therefore could easily go undetected.

11.4.5 Applications

The first application is to the full graben model in Fig. 11.18. The reference level is at the regional elevation of horizon 1. The points representing the pre-growth interval fall on a straight line because they all have the same displacement. The inverse slope of the best-fitting straight line (–4.5 units) is the total displacement on the lower detachment used to generate the model. The point at which the lost area goes to zero is the location of the lower detachment (–9.62 units below the reference level) which is the position of the lower detachment in the model. The growth beds (horizons 1–5) have lost areas that decrease upward. The lost area of the youngest growth bed is not zero because an increment of extension has occurred after the deposition of this unit. Layer-parallel strain is found with Eq. 11.27 and thickness changes by substituting the layer-parallel strains into Eq. 11.16. The pre-growth sequence is significantly stretched horizontally and thinned vertically by the deformation (Table 11.1), as is obvious on the cross section. The total displacements of the growth beds have been determined from Eq. 11.18 (Table 11.1), given the position of the lower detachment, and match the

Table 11.1. Structural data calculated from the full graben model in Fig. 11.18a (Groshong et al. 2003)

Unit top	Total displacement	Layer-parallel extension (%)	Layer-normal shortening (%)
1	1.0	+0.9	–0.9
2	1.5	+2.6	–2.5
3	2.5	+4.6	–4.4
4	3.0	+7.0	–6.5
5	4.0	+10.3	–9.3
6	4.5	+15.2	–13.2
7	4.5	+24.0	–19.4
8	4.5	+37.5	–27.3
9	4.5	+66.2	–39.8
10	4.5	+104.2	–51.0

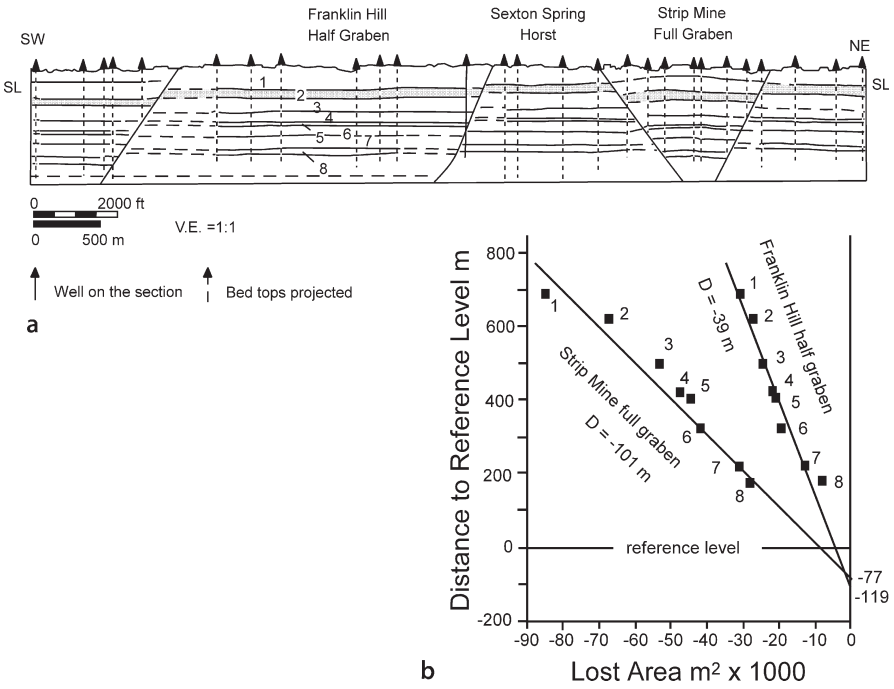

Fig. 11.21. Area-depth interpretation of the Deerlick Creek coalbed methane field. **a** Cross section perpendicular to fault strike showing the calculated lower detachment at the base of the section. The *dashed line* near the base of the section is the reference level. Units *1–8* are coal cycles. **b** Lost-area diagram for the Franklin Hill and Strip Mine grabens. S*olid lines* are the least-squares best fits; *V.E.:* vertical exaggeration. (Modified from Groshong 1994, after Wang 1994)

input values. The growth sequence includes depositional thickening which is greater than the structural thinning, giving a net thickness increase in each growth unit. The structural thinning (Table 11.1) can be recognized from the area balance (Eq. 11.27) in spite of the net thickness increase due to deposition.

A typical field application to an extensional structure is illustrated by a pair of grabens from the Pennsylvanian coal measures of the Black Warrior basin of Alabama. The cross section (Fig. 11.21a) is based on multiple horizons from closely spaced wells. Is this a valid cross section and how deep do the faults extend? The lost area is measured for each coal cycle boundary. The positions of the cycle boundaries at their footwall cutoffs coincide with regional dip across the area, from which it is inferred that footwall uplift is negligible. Lines joining the footwall cutoffs are therefore chosen as the regionals. The lost area for a given cycle boundary is the area bordered by the position of the boundary in the graben, the faults, and the regional for that cycle. The reference level was chosen to be at the base of the well control and parallel to regional dip. The distance from each regional to the reference level is measured in the center of each graben.

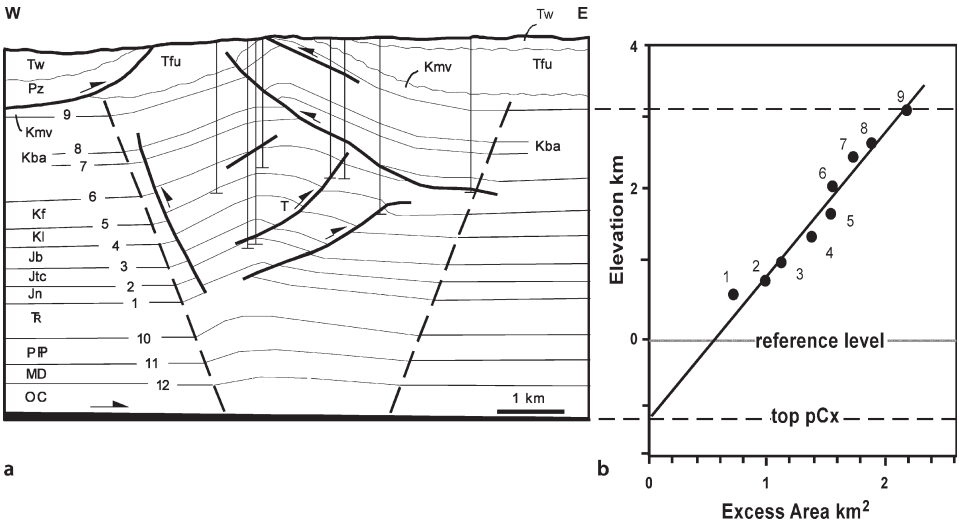

Fig. 11.22. Area-depth interpretation of the Tip Top anticline, Wyoming thrust belt, western U.S. **a** Cross section, areas below horizon 1 match the best-fit area-depth line (Groshong and Epard 1994, after Webel 1987). **b** Best-fit area-depth line (after Epard and Groshong 1993)

The area-depth curves for both grabens are straight lines with a modest amount of scatter (Fig. 11.21b). This amount of scatter is normal and so the section is validated. The best-fit lines go to zero area at depths below the reference level of –199 and –77 m, representing the predicted depths of the detachment. The agreement between the depths to detachment, calculated independently for two different grabens of different structural styles, is additional evidence of a valid result. The displacement on the lower detachment is 39 m for the Franklin Hill half graben and 101 m for the Strip Mine full graben.

The Tip Top anticline provides a field example of a compressional fold formed by shortening at the front of the Wyoming thrust belt (Fig. 11.22a). The upper part of the structure is constrained by surface geology and the wells but the deeper structure is open to question. Is the interpretation valid? The presence or absence of layer-parallel strain is unknown, as is the position of the lower detachment.

The data points from nine measurable horizons in the anticline fall reasonably close to the least-squares best-fit straight line $h = (1 / 0.51)\, S - 1.10$, with correlation coefficient 0.961 (Fig. 11.22b). This result validates the interpretation and indicates that the structure could be a locally balanced detachment fold (Sect. 11.4.3). The displacement on the lower detachment is 0.51 km. The depth of the basal detachment is 1.10 km below the reference level at the base of the Triassic. This places the lower detachment at the stratigraphic level of the top of the crystalline basement. The extrapolation of the section to the lower detachment in Fig. 11.22a is based on the area-depth line and shows the size of the structural closures predicted from the area-depth line for horizons 10–12 below the base of the Triassic.

11.5 Rigid-Body Displacement

This section begins the presentation of the kinematic-model-based restoration and prediction techniques. If all the deformation is by the displacement of rigid blocks, then a cross section can be restored by rigid-block translation and rotation. Rigid-body displacement preserves all the original lengths and angles within the blocks on the deformed-state cross section. This method is suitable for cross sections consisting of internally undeformed fault blocks, most commonly found in extensional structural styles. The sequential restoration of the Rhine Graben (Fig. 11.9) was done by rigid-body displacement.

11.5.1 Restoration

Rigid-body restoration can be done by cutting the cross section apart on the faults, removing the offsets, and reassembling it so that the reference horizon has the required restored shape. An analogous strategy works with computer-drafting programs. The restoration can be done on paper without cutting by tracing the blocks on a transparent overlay (Fig. 11.23). Draw the pin line, the restored-bed reference line, and the footwall on the transparent overlay. Move the overlay so that the first block is in its restored position and trace it onto the overlay. Then move the overlay so that the second block is in the restored position and trace it. Repeat this step until the section has been restored. If the blocks do not fit together perfectly, it is preferable to leave gaps between them, rather than to overlap the blocks.

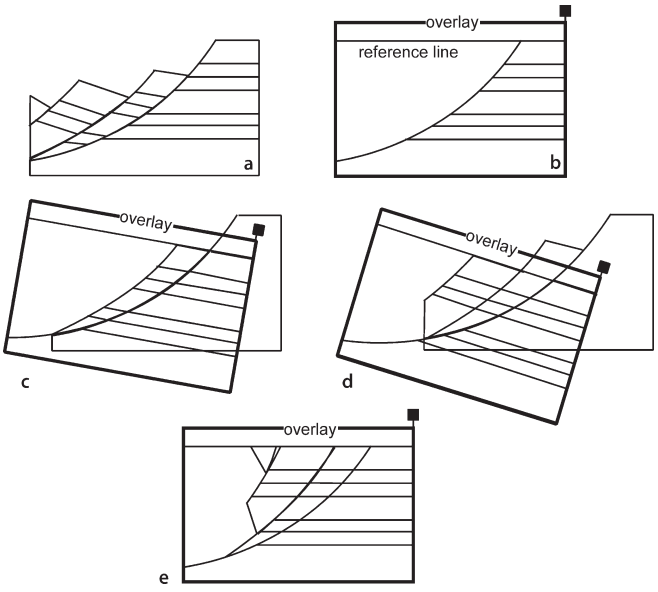

Fig. 11.23. Restoration of rigid-body displacement by the overlay method. **a** Section to be restored. **b** Preparation of the overlay. **c** Restoration of the first block. **d** Restoration of the second block. **e** Complete restoration

11.5.2
Domino-Block Predictive Model

Dominoes are formed by parallel planar faults for which both bedding and the faults rotate (Fig. 11.24). Found typically in extensional and wrench regimes, the amount of rotation may be large, 30° to 60° or more. Such large rotations by other models require very large internal strains and seem not to be favored. This was one of the first kinematic models to be quantified (Thompson 1960; Morton and Black 1975). As the blocks extend, they rotate. Following the approach of Wernicke and Burchfiel (1982), the relationship between the extension and the geometry is

$$e = [\sin(\phi + \delta) / \sin\phi] - 1 \quad , \tag{11.37}$$

where ϕ = the final dip of the fault, δ = the final dip of bedding. The initial dip of the fault is $\phi_0 = \phi + \delta$ allowing Eq. 11.37 to be rewritten as

$$e = [\sin\phi_0 / \sin(\phi_0 - \delta)] - 1 \quad . \tag{11.38}$$

The slip on the fault depends on the width of the fault block, the wider the block, the greater the slip on each block. The fault slip is (Axen 1988)

$$S_r = L_0 \sin\delta / \sin\phi \quad , \tag{11.39}$$

where S_r = rotational fault slip and L_0 = the original horizontal distance between two adjacent faults. The rotational slip is calculated using the L_0 value of the hangingwall block.

The correct frame of reference for calculating domino block strain is the median line through the blocks or, equivalently, the enveloping surfaces that touch the corners

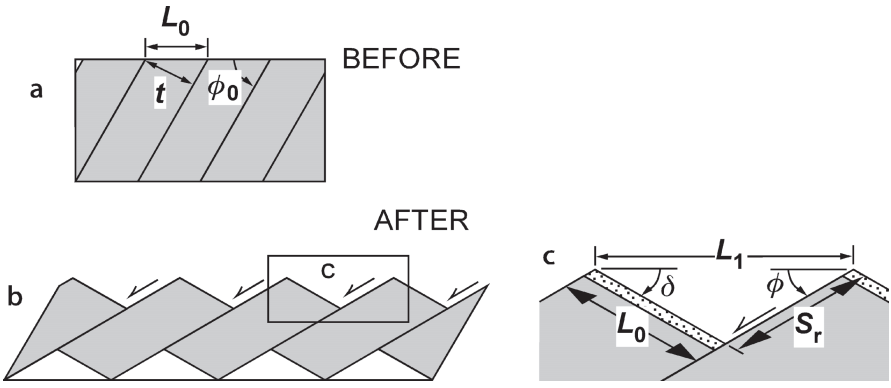

Fig. 11.24. Domino kinematics and strain (after Axen 1988). L_0: The original horizontal distance between two adjacent faults; L_1: final horizontal distance between two adjacent faults; ϕ_0: initial dip of the fault; ϕ: final dip of the fault; δ: final dip of bedding; S_r: slip on fault. **a** Before extension. **b** After extension. **c** Relationship among variables

of the blocks (Fig. 11.25a,b). Otherwise, external rotations can greatly change the amount of strain inferred from the domino geometry. To show the potential pitfall, an original set of domino blocks (Fig. 11.25a) is stretched 18.3% (Eq. 11.37, Fig. 11.25b), then rotated 15°. A counterclockwise external rotation of the stretched dominoes of 15° (Fig. 11.23c) produces horizontal bedding and faults having their original dips. According to Eq. 11.37, using a horizontal reference line, the domino strain would be zero because the bedding and faults are not rotated. From a median surface reference line, the strain remains 18.3%. A 15° clockwise rotation of the dominoes (Fig. 11.25d) increases the bedding dip and decreases the fault dip with respect to the horizontal

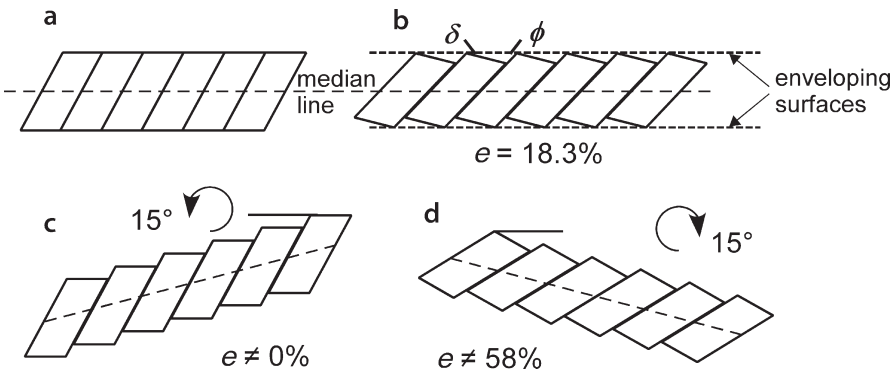

Fig. 11.25. Effect of external rotation on strain inferred from domino block geometry **a** Unrotated dominoes. **b** Internal rotation of domino blocks, without external rotation, 18.3% extension. **c** 15° counterclockwise rotation of **b**. **d** 15° clockwise rotation of **b**

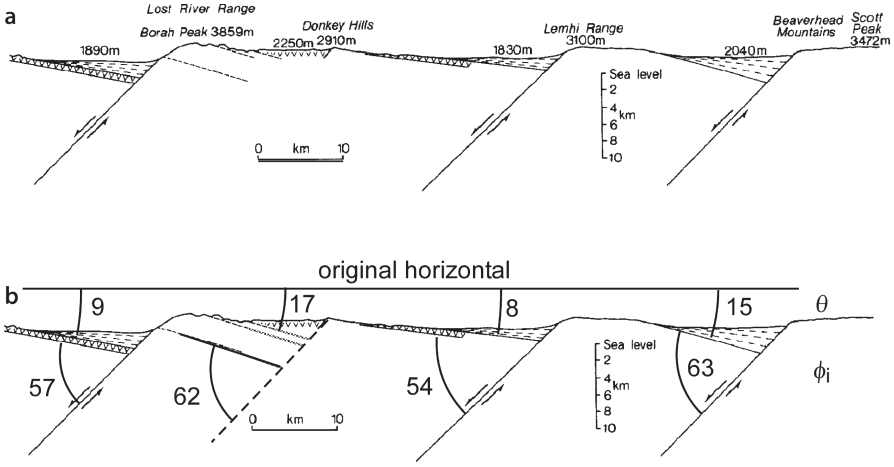

Fig. 11.26. Domino model applied to example in Basin and Range Province of the western U.S. **a** East-west cross section from the Wasatch fault to Bear Lake, about 100 km north of Salt Lake City, Utah (after Westaway 1991). **b** Measurements for domino-model strain calculation

and thereby greatly increases the amount of strain (to 58%) given by Eq. 11.37 using horizontal as the reference line. Again, using the median line as the reference, the strain is 18.3%.

Seismically active faults in the Basin and Range province of the western U.S. provide an example of domino-block deformation. The faults are planar and steeply dipping to depths of at least 10 km, breaking the crust into a series of dominoes (Fig. 11.26). How much crustal extension is implied by the geometry of the dominoes? The extension can be found from Eq. 11.38 and the measurements shown in Fig. 11.26b. Because the cutoff angles are different for each block, so are the extension strains. The horizontal extension is, from the left domino to the right domino, 12.9%, 24.9%, 12.5%, and 19.9%. Rigid dominoes should rotate the same amount and so the different amounts of rotation and the different strain magnitudes could be viewed as representing departures from perfect rigid-block deformation.

11.5.3 Circular-Fault Predictive Model

Circular-arc faults permit rigid rotation of the hangingwall block. Rarely are faults complete circular arcs, but the upper part of a listric thrust may be approximately circular. Quantitative kinematic models for block rotation on listric thrusts have been developed for and successfully applied to normal faults (Moretti et al. 1988) and basement-involved thrust faults (Erslev 1986, 1993; Seeber and Sorlien 2000). The model below is for a listric thrust fault. It allows the prediction of the location of the lower detachment and the displacement from the fault dip and the width of the structure.

The kinematic model (Fig. 11.27) is based on a fault that is a segment of a circular arc with radius R from a center C. The circular portion of the fault meets the planar

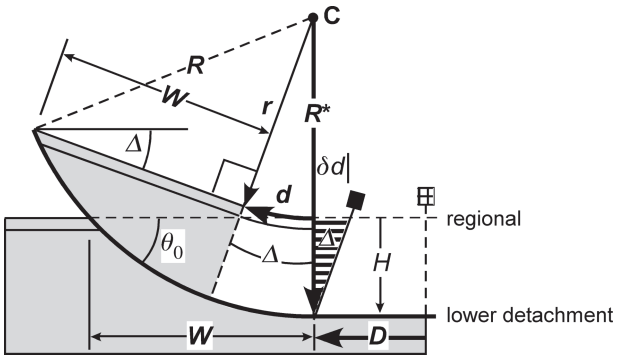

Fig. 11.27. Kinematic model of a rotated block above a circular-arc thrust. The hangingwall is displaced D along the lower detachment. *Light shading* is rigid; *Δ:* rotation angle; *R:* radius of curvature; *C: center of curvature; R*: radius on a line orthogonal* to the regional; θ_0 is the dip at the fault at regional; *d:* displacement of a marker at a distance r from the center of curvature; *W:* width of the structure at regional; *H:* depth to detachment from the regional. The *dashed pin line* is the original trailing edge. The *solid-head pin* is the trailing edge of a constant-bed-length structure; δd is the length imbalance with respect to a vertical trailing edge

lower detachment along the radius R^*, orthogonal to the regional, located where the hangingwall marker bed in the anticline returns to regional dip. Rigid-block rotation is possible for the main part of the hangingwall (shaded, Fig. 11.27). The original dip of the fault at regional is θ_0, which, together with the width of the structure, W, is a function of the radius of curvature, r, of the marker bed

$$r = W / \tan \theta_0 \quad . \tag{11.40}$$

The center of curvature of the fault is located a distance r above the regional along R^*. If the dip of the fault at regional is not visible, then it can be found from the dip of the fault at its tip, θ_1, from

$$\theta_0 = \theta_1 - \Delta \quad , \tag{11.41}$$

where Δ dip of the fault block. Once r and W are known, the radius, R, to the detachment from the center of curvature is

$$R = (W^2 + r^2)^{1/2} \quad . \tag{11.42}$$

The depth to the lower detachment from the regional is H, where

$$H = R - r \quad . \tag{11.43}$$

The displacements are

$$d = r\ \Delta / 57.3 \quad , \tag{11.44}$$

$$D = R\ \Delta / 57.3 \quad , \tag{11.45}$$

where d = displacement at the level of the regional datum, D = displacement on the lower detachment, and Δ is in degrees.

Total rigid-block rotation is impossible because the trailing edge of the rotated block (unshaded, Fig. 11.27) moves from a planar lower detachment onto the curved ramp, requiring some form of internal deformation. If the original hangingwall remains rigid, the displacement increases downward toward the detachment. To maintain constant bed length and bed thickness behind the rigid block, flexural slip is required and would cause the trailing pin line to rotate (solid head, Fig. 11.27). The magnitude of the slip is

$$\delta d = D - d = H \tan \Delta \quad . \tag{11.46}$$

The final geometry of the trailing pin line is of great importance. If the pin line rotates to maintain constant bed length and bed thickness, as shown by the solid-head pin in Fig. 11.27, then the rotated block will impose regional layer-parallel shear on the hinterland of the structure. Mechanically it seems much more likely that displacement of the hinterland block will be approximately constant, which requires that

the trailing edge remain vertical in the deformed state. This leads to a second reason why perfect rigid-block rotation with the geometry of Fig. 11.27 is unlikely: it is not length or area balanced with a vertical pin line. The length imbalance is δd (Eq. 11.46). The area imbalance is equal to the area, A, of the triangle bounded by H and δd,

$$A = (H^2 \tan \Delta)/2 \quad . \tag{11.47}$$

Thus it is unlikely that the hangingwall will maintain constant length and thickness, but instead it is likely to deform internally in some fashion in order to remain locally balanced.

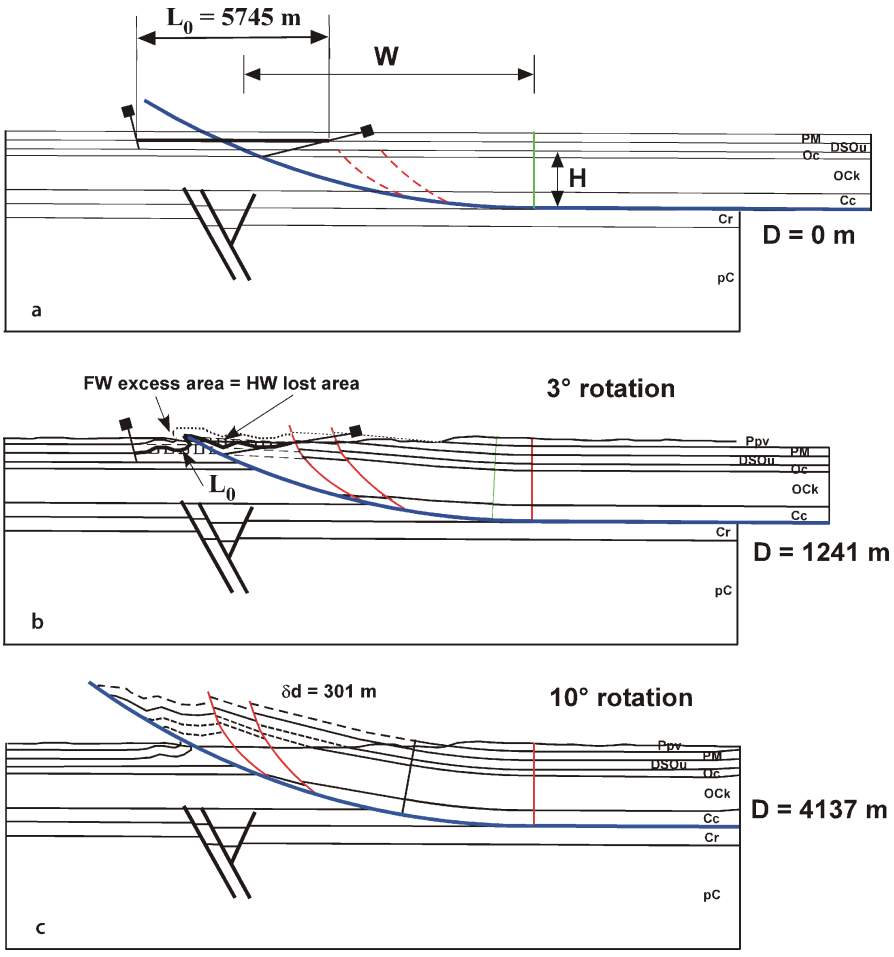

Fig. 11.28. Model-based sequential restoration of Wills Valley anticline. *D:* displacement on lower detachment. **a** Undeformed. **b** After 3° rotation of hangingwall, just before master fault breaks across PM. *Shading* shows area transferred from hangingwall to footwall. **c** After 10° rotation of hangingwall into present day configuration. Everything above the erosion surface is schematic, based on the model

The Wills Valley anticline provides an example of rigid-block rotation above a circular-arc thrust and of a model-based sequential restoration. The cross section is from the middle of an approximately 140 km long, straight, anticline located in the frontal part of the southern Appalachian fold-thrust belt. The cross section on which Fig. 11.28c is based is derived from outcrop geology and a seismic reflection profile (Fig. 1.46). This structure fits a circular-block model with best-fit measurements of $\Delta = 10°$, $W = 8.88$ km and $\theta_0 = 22°$. From Eqs. 11.40, 11.42, and 11.43, respectively, $r = 21.98$ km, $R = 23.7$ km, and $H = 1.73$ km. From Eq. 11.45, the displacement that produced the structure is $D = 4.137$ km. These values allow the structure to be restored to zero displacement (Fig. 11.28a), from which the bed lengths are measured and included in Fig. 11.28c. From Eqs. 11.46 and 11.47, respectively, $\delta d = 301$ m, and $A = 5.3 \times 10^5$ m^2. These values are included in Fig. 11.28c with the displacement accommodated by the hangingwall splay thrusts and the excess area accommodated by the uplift on the splays.

A footwall syncline is preserved beneath the master thrust indicating a fault-tip fold was once present, which is reconstructed in Fig. 11.28b. The outer limits of the region inferred to be affected by fault-tip folding are indicated by the pin lines shown in Fig. 11.28a,b. The outer limit of folding on the footwall is obtained directly from the cross section. The outer limit of folding on the hangingwall is somewhat arbitrary because the fold has been eroded from the hangingwall. The pin is placed at the hangingwall cutoff of the top OCk, which is appears not to be folded, and is sloped sharply outward to include comparable widths of PM in the hangingwall and footwall, giving a length L_0 of 5 745 m at the base of the PM. If L_0 is too short, the necessary area cannot be obtained on the hangingwall; if it is too long, an unrealistic amount of the hangingwall is folded. The reconstruction of Fig. 11.28b is constrained by the known geometry of the footwall folds, area balance, and maintaining constant bed length at the base of the PM. A 3° rotation of the hangingwall and attendant displacement causes the straight-line distance between the endpoints of L_0 to be reduced to 4 751 m. These constraints require folding on the hangingwall as well as the footwall. For a 3° rotation, δd at the top of the Cc is 117 m (Eq. 11.46) and the excess area required to maintain a vertical trailing pin line is $A = 1.6 \times 10^5$ m^2 (Eq. 11.47). These values are incorporated into the geometry of the hangingwall as displacement and thickening on the splay faults and their hangingwalls.

11.6 Flexural-Slip Deformation

Flexural-slip restoration is based on the model that bed lengths do not change during deformation (Chamberlin 1910; Dahlstrom 1969; Woodward et al. 1985, 1989). Internal deformation is assumed to occur mainly by layer-parallel simple shear (Fig. 11.3b). For the area to remain constant, the bed thicknesses must be unchanged by the deformation as well. This is the constant bed length, constant bed thickness (constant BLT) model. Flexural-slip restoration is particularly suitable where the beds are folded and structurally induced thickness changes are small, the style of deformation in many compressional structures. Flexural slip is also commonly used to restore the complex deformation above salt layers (Hossack 1996).

11.6.1 Restoration

Flexural-slip restoration consists of measuring bed lengths and straightening the lengths while preserving the thicknesses to produce the restored section. The section to be restored is bounded on one end by a pin line and on the other by a loose line (Fig. 11.29). The pin line is a straight line on the deformed-state cross section that is required to remain straight and perpendicular to bedding on the restored section. The loose line is a straight line on the deformed-state section that may assume any configuration on the restored section, as required by the restoration. For the sake of clarity, pin lines are shown here as having solid heads and loose lines as having open heads.

A loose line that is straight and parallel to the pin line is the best indication of a valid restoration (Fig. 11.29b). Faults on the deformed-state cross section are shown in their restored positions on the restored section (Fig. 11.29b). The reasonableness of the restored shape of the fault is another criterion for the quality of the restoration. Note that the lengths of lines oblique to bedding and the cutoff angles between bedding and faults are changed by the deformation and so are different in the deformed-state and restored cross sections. A loose line that is highly irregular is the clearest indication of a section that is not valid (Fig. 11.30a). A straight but inclined loose line (Fig. 11.30b) indicates a systematic length difference that may represent an invalid cross section, a poor choice of the pin line or the loose line, or material introduced or removed by layer-parallel simple shear. Usually at least four to five beds must be tested to determine whether the section is correctly restorable or if some type of error is present.

In complex structures, the choice of pin line and loose line requires care. The goal is to choose the pin line and loose line in locations that can be expected to restore to perpendicular to bedding and consequently to have constant bed lengths between them. There are a number of possible choices. The best location for a pin line and loose line

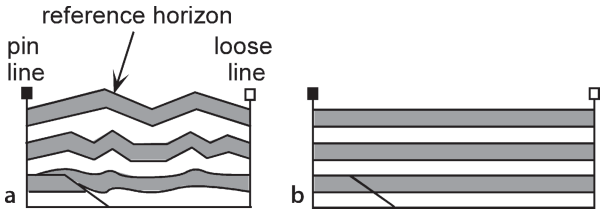

Fig. 11.29. Cross-section restoration. *Pin line*, solid-head; *loose line*, open-head. **a** Deformed-state cross section. **b** Restored section: equal bed lengths and a *straight loose line* indicate a satisfactory restoration

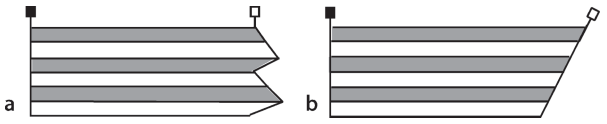

Fig. 11.30. Imperfect restorations. **a** *Irregular loose line* indicates an invalid section. **b** Systematic error: the *linear loose line* may indicate an invalid section or a poor choice of pin line or loose line

is in undeformed beds adjacent to the area of interest, but such locations may not be available. Often both the pin line and the loose line must be placed in deformed beds. Some of the better possibilities are

1. Along an axial surface. This is appropriate for fixed-hinge folds in which shear does not occur across the axial surfaces.
2. Perpendicular to horizontal beds. This is appropriate if the strain is zero or constant where beds are horizontal.
3. Pin line and loose line located where the dip is the same in amount and direction. This is appropriate where layer-parallel shear is proportional to dip.

The typical result of an incorrect choice of a pin line or loose line is the systematic length error shown by a straight but inclined loose line (Fig. 11.30b). A systematic error might be corrected by a better choice of pin line and/or loose line without any changes to the cross section itself.

To restore a structure, the pin line and loose line are chosen (Fig. 11.31a), and the bed lengths are measured between them, stretched out and placed on the restoration (Fig. 11.31b). Lengths may be measured by a variety of means. Chamberlin (1910) used a thin copper wire, curved to follow bedding, then straightened. A ruler or a straight piece of paper can be rotated along the contact, the lengths of many small segments marked, and the total measured at the end. Computer methods are especially quick and convenient (Groshong and Epard 1996). Thicknesses in the deformed-state are preserved on the restored cross sections. Faults are drawn on the restored cross section in the positions required by the restored bed lengths. The restored fault trajectories should match those expected for the structural style. Ordinarily faults should restore to planes, smooth curves, or ramp-flat geometries.

A question that must be addressed with any restoration is how straight must the loose line be in order to represent a valid cross section? The loose line in Fig. 11.31b is not perfectly straight, but the cross section can be considered valid for most purposes. Constant BLT line-length restoration is a robust technique for which small violations of the constant BLT assumption cause only small effects in the restoration. The lower, shorter part of the loose line in Fig. 11.31b may be caused by a small amount of layer-parallel shortening and thickening of the units in the inner arc of the physical model. Discrepancies that clearly indicate an invalid cross section are large (Fig. 11.32). Wilkerson and Dicken (2001) provide an excellent review of common problems revealed by the restoration of thrust faults along with appropriate corrective measures.

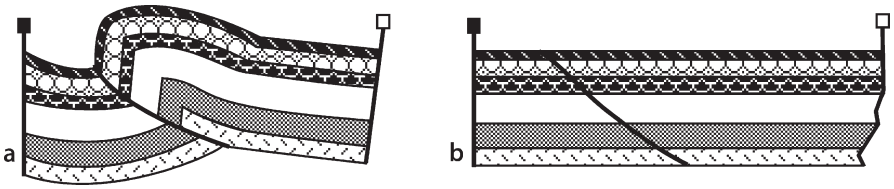

Fig. 11.31. Flexural-slip restoration of the cross section of a physical model. **a** Deformed-state section. **b** Restored section. (After Kligfield et al. 1986)

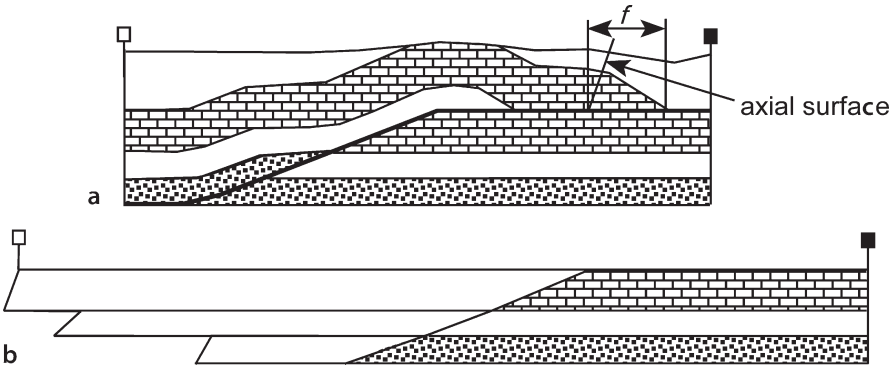

Fig. 11.32. Flexural-slip restoration of an invalid cross section. **a** Deformed-state cross section. Preserved beds maintain constant bed thickness (after a problem in Woodward et al. 1985). *f:* hangingwall fault ramp. **b** Flexural-slip restoration based on length measurements at the top and base of each unit

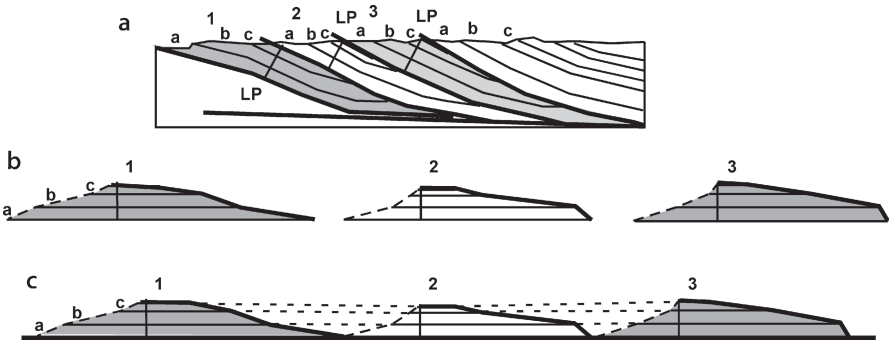

Fig. 11.33. Restoration using local pin lines (after Woodward et al. 1989). **a** Deformed-state cross section of eroded thrust sheets. *LP:* local pin line; *1–3:* thrust sheets; *a–c:* stratigraphic units. **b** Thrust sheets individually restored from local pin lines. **c** Thrust sheets restored to minimum displacement positions. *Dashed lines* are eroded beds

A simple measurement pitfall to avoid is including a fault length with the bed length. In Fig. 11.32a, a portion of the base of the limestone is a fault ramp (f) where the bedding is truncated against the upper detachment. The fault ramp segment is not part of the bed length of the base of the limestone. The fault ramp is separated from unfaulted bedding by an axial surface which, in the case of constant bed thickness, bisects the associated fold hinge (Sect. 6.4.1). Splitting the limestone bed by drawing many parallel beds within the unit would make the fault cutoffs, and hence the ramp, obvious.

Local pin lines (Fig. 11.33) should be used where erosion or lack of information renders the connection between hangingwall and footwall uncertain. A local pin line is placed in each block and the beds stretched out in both directions from the local pin. The individual restored blocks can then reassembled by bringing the individual blocks as close together as geologically appropriate.

A stratigraphic template (Woodward et al. 1989) greatly speeds up the reconstruction process for beds having uniform thickness or a constant thickness gradient. The template is a series of lines representing the restored bed geometry. For constant bed thickness the lines are parallel. A constant bed-length restoration can then be done by measuring bed lengths and marking the appropriate lengths on the template. This saves the time of drawing each bed segment separately. Regional thickness gradients can be shown on the template by diverging lines.

Units that have primary stratigraphic thicknesses changes may be restored by a modification of the constant line-length method. Begin with the uppermost unit that is to be restored, the top of which is the reference horizon. The thickness of this unit is measured at multiple points along the layer (Fig. 11.34a). The positions of the thickness measurements are recorded with respect to the pin line on the top of the unit. The top of the unit is restored and the distances of the thickness measurement points from the pin line are marked. The thicknesses are marked on the restoration in the direction perpendicular to the upper horizon (Fig. 11.34b). The lower horizon is drawn to maintain its original length but it may "slip" laterally past the points where the thickness was measured. The restoration preserves the lengths between segments on the base of the unit but not necessarily their positions. The total line length is preserved on the top and base. For a section containing faults (Fig. 11.34c,d), thickness measurements are taken at fault cutoffs and restored with respect to the upper cutoff if possible, otherwise with respect to the lower cutoff. Each stratigraphic unit on the cross section is measured and restored separately to the base of the unit above it until the restoration is complete.

Difficulties may be encountered in piecing the section back together across faults. The problems are usually related to uncertainty in the correct restoration of the fault shape. The best solution is to subdivide the stratigraphy into thinner units and then restore the thinner units as just described. In the limit, each unit being restored is a single line of variable thickness that is stretched out and placed along side the unit above it.

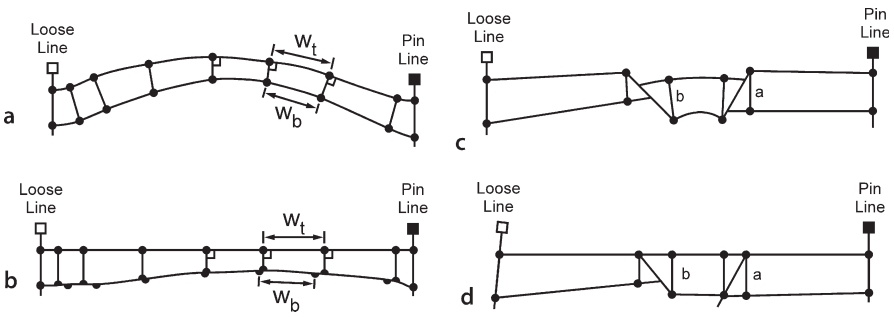

Fig. 11.34. Bed-length restoration of variable thickness units (after Brewer and Groshong 1993). *Dots* represent points at which original thickness measurements are made. W_t: segment width at top; W_b: segment width at base. **a** Deformed state fold. **b** Restored fold. **c** Deformed-state faulted fold. **d** Restored faulted fold

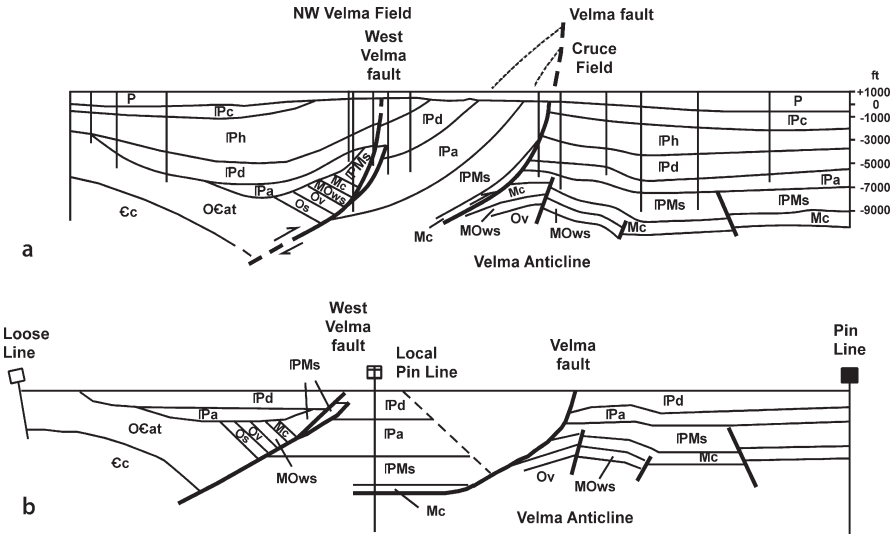

Fig. 11.35. Northwest Velma and Cruce oil fields. **a** Cross section based on wells and a seismic line (redrawn from Perry 1989). *P:* Permian red sand and shale; *Pc:* Cisco Group; *Ph:* Hoxbar sand, shale and limestone; *Pd:* Deese sand, shale and limestone; *Pa:* Atoka Formation; *PMs:* Springer sand and shale; *Mc:* Caney shale; *MOws:* Woodford shale, Hunton limestone and Sylvan shale; *Ov:* Viola limestone; *Os:* Simpson Gp. including Bromide and Oil Creek sands; *OCat:* Arbuckle Gp. limestone and Timbered Hills Gp. limestone and sandstone; *Cc:* Carlton Rhyolite. **b** Flexural-slip restoration

A cross section of a convergent-wrench structure from central Oklahoma provides an example of flexural-slip restoration where variable stratigraphic thicknesses are to be preserved (Fig. 11.35a). The section is located across the down plunge extension of the Wichita uplift, a basement cored anticline demonstrated by McConnell (1989) to be a convergent wrench-fault structure. The presence of folding as well as faulting suggests that the flexural-slip restoration technique is appropriate, as modified for variable original bed thickness. The pin line is placed in the horizontal beds on the right side of the cross section and the top of the Pd is restored to horizontal. The restoration proceeds to the left and downward from the pin line in the uppermost bed. The Velma fault is a major discontinuity in bed thickness and so the restoration from the pin line is stopped at the fault. A local pin line is placed perpendicular to bedding in the hangingwall of the Velma fault and the restoration continued to the left. The restoration (Fig. 11.35b) is good, indicating that the cross section is valid and, in addition, provides information about the geological evolution. The restoration is geometric, not palinspastic. The Velma fault marks a significant stratigraphic discontinuity on the restored section, as would be expected if it has an unrestored strike-slip component. Some amount of unrestored vertical-axis rotation of the cross section is also possible (c.f., Sect. 11.2.2). Restoration to the top Pd removes the displacement on the Velma fault but preserves the Velma anticline and the West Velma fault, showing that they formed earlier.

11.6.2 Fault Shape Prediction

Based on the assumption of constant BLT on a cross section bounded by vertical pin lines, there is a unique relationship between the hangingwall shape caused by movement on a fault and the shape of the fault itself. In the technique developed by Geiser et al. (1988), a complete deformed-state cross section is constructed while simultaneously producing a restored cross section. The method is based on: (1) constant bed length and bed thickness, (2) slip parallel to bedding, (3) fixed pin lines in the hangingwall and footwall of the fault, and (4) the hangingwall geometry is controlled by the fault shape. The pin lines are chosen to be perpendicular to bedding. The data required to use the method are the location of a reference bed and the hangingwall and footwall fault cutoff locations of the reference bed. The original regional of the reference surface is not required. The method produces a cross section that is length balanced, has constant bed thickness and has bedding-normal pin lines at both ends.

The technique is as follows:

1. Define the reference bed, its fault cutoffs, and the shape of the fault between the cutoffs (Fig. 11.36a, top).
2. Place the pin lines in the deformed-state cross section. Usually they are chosen to be perpendicular to bedding and beyond the limits of the structure of interest (Fig. 11.36a, top).
3. Measure the bed length of the reference horizon between the pin lines and draw the restored-state section (Fig. 11.36a, bottom).
4. Construct one or more constant thickness beds in the hangingwall between the hangingwall pin and the fault (Fig. 11.36b, top).

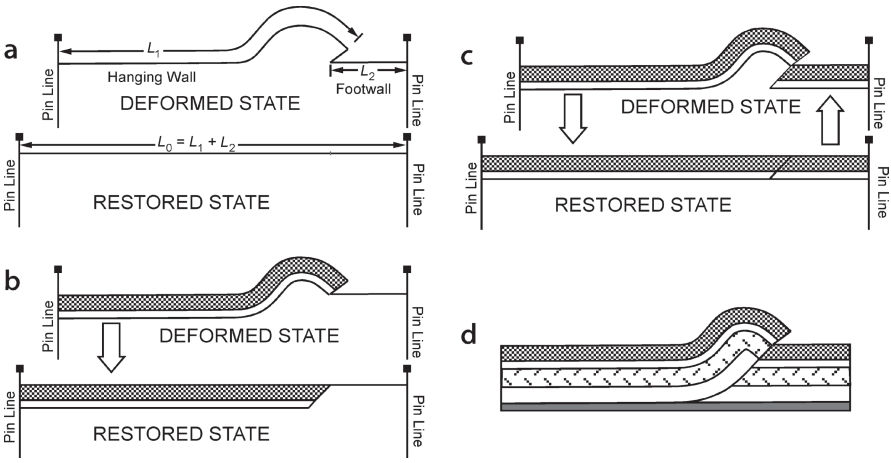

Fig. 11.36. Construction of fault shape from a hangingwall bed based on the constant BLT assumption (Geiser et al. 1988). **a** Initial geometry. **b** After first cycle of construction, hangingwall is restored. **c** After the first cycle of hangingwall restoration, the footwall is restored. **d** Completed cross section

5. Measure all the bed lengths in the hangingwall between the hangingwall pin and the fault and place them on the restored-state cross section (Fig. 11.36b, bottom). This defines the shape of the footwall beds in the restored state.
6. Draw the restored-state footwall on the deformed-state cross section (Fig. 11.36c, top). This gives a new hangingwall cutoff.
7. Continue the cycle of steps 4–6 until the section is complete (Fig. 11.36d).

This predictive technique is sensitive to the constant BLT assumption. Like the classical depth-to-detachment calculation (Sect. 11.4.2), small bed length changes will have a significant effect on the predicted depth to detachment. It is always best to confirm the predicted fault shape with additional information.

11.6.3 Flexural-Slip Kinematic Models

Numerous models have been developed that relate fold shape to fault shape for various flexural-slip structural styles. Many of these have adopted planar or ramp-flat fault shapes, leading to dip-domain cross-section styles (Sect. 6.4.1). Models like the fault-bend fold, fault-propagation fold and fault-tip fault-propagation fold of Fig. 11.37a–c are based on the assumption of constant bed length and constant bed thickness throughout and so yield unique relationships between the fold shape and the fault shape. Such models can be used to predict the entire structure from a very small amount of hard data. Other models, like the simple-shear, pure shear, and detachment folds in Fig. 11.37d–f, maintain constant BLT in the upper part of the structure but are area balanced in the decollement zone at the base. The latter style of model admits a wider range of geometries and so more must be known before the complete structure can be predicted. Other variants allow thickness changes in the steep limb, which creates even more degrees of freedom in the interpretation. A discussion of all the models and their variants is beyond the scope of this book. The objective here is to introduce the basic concepts and provide a guide to additional sources of information.

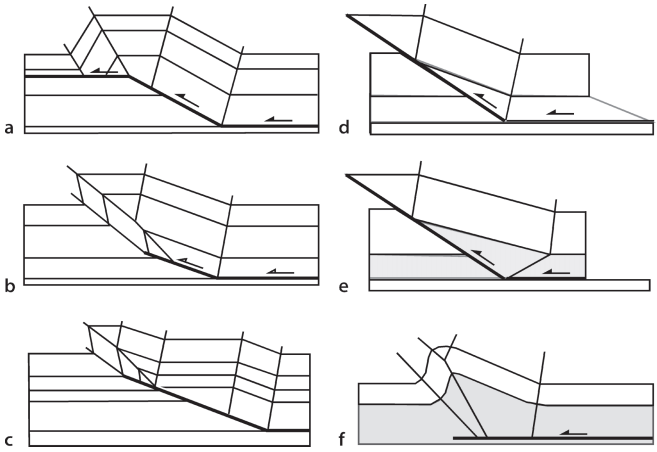

Fig. 11.37.
Fault-related fold models. *Unshaded:* constant-thickness units; *shaded:* variable-thickness unit. **a** Fault-bend fold (after Suppe 1983). **b** Fault-propagation fold (after Suppe 1985; Suppe and Medwedeff 1990). **c** Fault-propagation fold at the tip of a long ramp (after Chester and Chester 1990). **d** Simple-shear fault-bend fold (after Suppe et al. 2004). **e** Pure-shear fault-bend fold (after Suppe et al. 2004). **f** Detachment fold (after Jamison 1987)

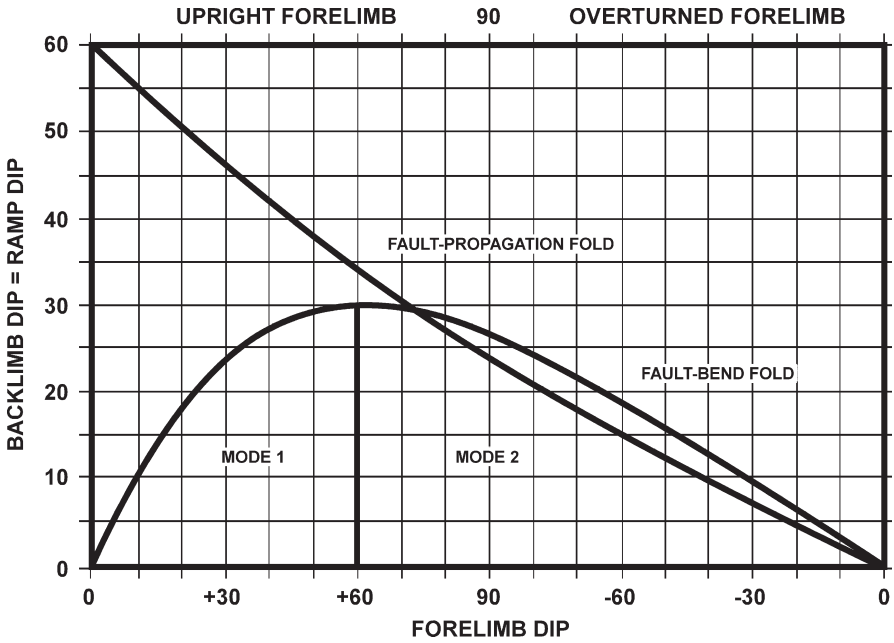

Fig. 11.38. Graph of forelimb vs. backlimb dips in constant bed thickness fault-bend and fault-propagation folds (Fig. 11.37a,b). The backlimb is always above the ramp

The starting point for a model-based interpretation is to determine which model is appropriate. Constant BLT fault-bend and fault-propagation folds have analytical relationships between forelimb and backlimb dips that can be expressed graphically. The graph (Fig. 11.38) is a plot of forelimb dip versus backlimb dip, with the dips being measured relative to the regional dip outside the fold. A field example can be plotted on Fig. 11.38 to see if falls on either the fault-bend or fault-propagation fold curve. If the point falls on one of the lines, then there is a high probability that the fold fits the model and the model can be used to predict the fold geometry.

As an example of the methodology, the deep structure of the fold in Fig. 11.39a is interpreted. The regional dip is inferred to be parallel to the planar domain between the two limbs and is confirmed because the same dip is seen outside the structure. The limb dips are measured with respect to regional Fig. 11.39a and plotted on Fig. 11.38, The points fall on the fault-bend fold curve, indicating the model to be used. In Fig. 11.39b the interlimb angles are measured and bisected to find the axial-surfaces. The backlimb axial surfaces (1 and 2) are parallel, as are the forelimb axial surfaces (3 and 4). Beds must return to regional dip outside the anticline, allowing the location where the forelimb flattens into regional dip (axial surface 4) to be determined. The fault ramp must be below and parallel to the backlimb (Fig. 11.39c). The exact location of the fault requires additional information about the position of the lower and upper detachments. Bed truncations in the forelimb of the hangingwall or against the ramp

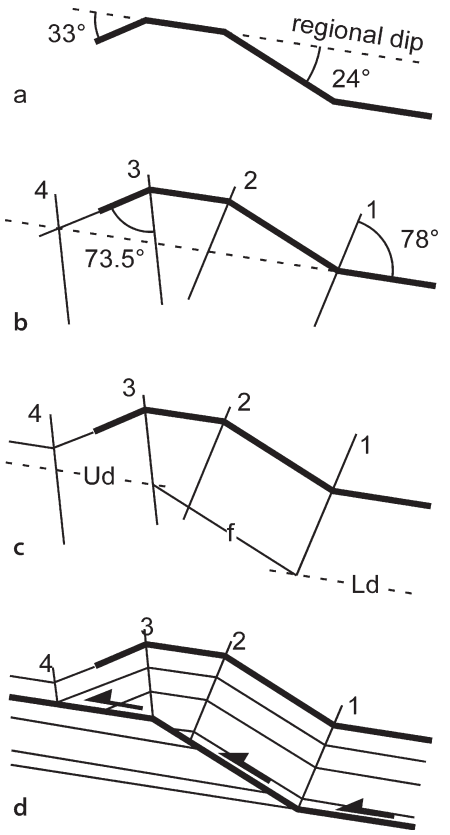

Fig. 11.39.
Construction of a complete fault-bend fold starting with a single horizon. **a** Starting fold geometry with dips measured from regional dip. **b** Axial surfaces bisect hinges. **c** Location of the fault. *Ud:* upper detachment; *f:* fault ramp; *Ld:* lower detachment. **d** Final geometry

in the footwall may serve to locate the detachments. Alternatively, the stratigraphic section may contain known detachment horizons that can be utilized in the interpretation. Additional controls from the model are that axial surfaces 1 and 2 always terminate at the upper detachment, and axial surface 1 always terminates at the base of the ramp. Axial surface 3 can be on the ramp or at the top of the ramp. Having determined the best location for the fault, the dip domains can be filled in with the appropriate stratigraphy (Fig. 11.39d) and the interpretation is complete.

Since the pioneering work by Suppe (1983), there have been numerous papers describing models for flexural-slip fault-related folds. The following is a representative list of significant papers on the topic: Jamison 1987; Chester and Chester 1990; Mitra 1990; Suppe and Medwedeff 1990; Jordan and Noack 1992; Suppe et al. 1992; Mitra 1993; Epard and Groshong 1995; Homza and Wallace 1995; Wickham 1995; Poblet and McClay 1996; Poblet et al. 1997; Medwedeff and Suppe 1997; Suppe et al. 2004. The recent book by Shaw et al. (2005) is an excellent discussion of the application of models to compressional structures. Predictions based on 3-D axial-surface geometry are described by Shaw et al. 2005b and Rowan and Linares 2005).

11.7 Simple-Shear Deformation

According to the simple-shear concept, a cross section deforms as if it were made up of an infinite number of planar slices that are free to slip past one another (Fig. 11.40). The shear direction is specified as having a dip α with respect to a regional that does not change during deformation. The special case for which the shear plane makes an angle of 90° to the regional is called vertical simple shear because the regional is usually horizontal (Fig. 11.40a). Oblique simple shear is simple shear along planes at some angle other than perpendicular to the regional (Fig. 11.40b, $\alpha \neq 90°$). (Some workers measure α from the vertical.) Simple-shear restoration is most widely used for extensional structures, in particular the hangingwall rollovers associated with half grabens.

11.7.1 Restoration

11.7.1.1 Vertical Simple Shear

Restoration by vertical simple shear involves the differential vertical displacement of vertical slices of a cross section to restore a reference horizon to a datum (Verrall 1982). This method has its origins in the well-log correlation technique in which the logs are slipped vertically until aligned side-by-side along an easily recognized marker horizon. The alignment makes the correlation of nearby markers much easier. Many computer programs designed for geological or geophysical data interpretation implement a function of this type. Folds and growth stratigraphy are easily restored by this method. The restoration of dipping beds by vertical simple shear preserves vertical (isocore) thicknesses but changes the stratigraphic thicknesses and the bed lengths.

Begin a vertical simple-shear restoration by picking the reference horizon to be flattened. In the example of Fig. 11.41a, the top of the sandstone is selected to be the reference horizon. Define the individual elements to be displaced (lithological logs in this example). Restore the cross section by shifting the elements vertically until the

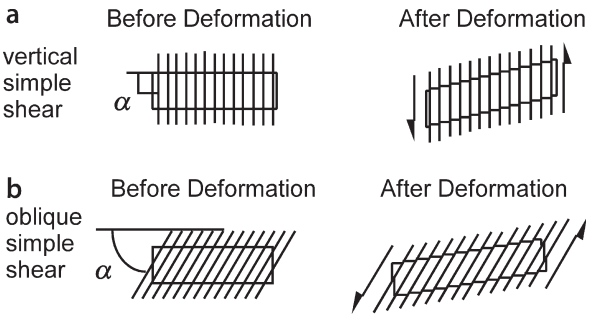

Fig. 11.40. Simple shear oblique to bedding. **a** Vertical simple shear. **b** Oblique simple shear

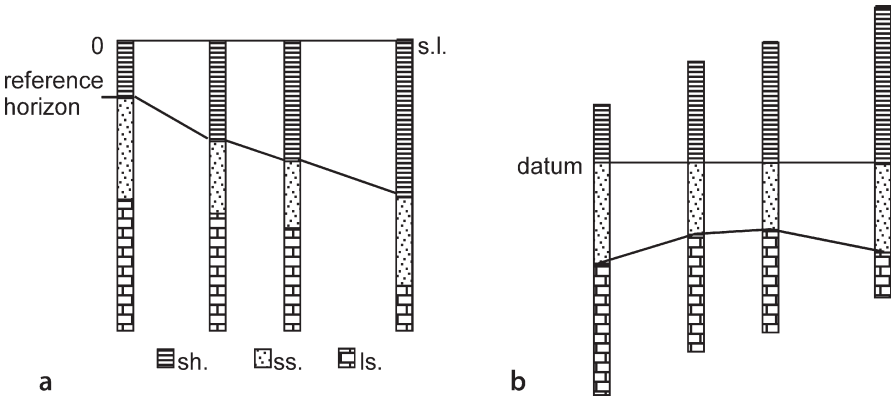

Fig. 11.41. Flattening to a datum by vertical simple shear. **a** Deformed-state cross section based on lithological logs. The zero elevation is sea level (*s.l.*); *sh:* shale; *ss:* sandstone; *ls:* limestone. **b** Cross section flattened to a datum at the top of the sandstone shows a paleo-anticline at the top of the limestone

reference horizon is horizontal (Fig. 11.41b). The operations required to restore the cross section may be easily performed by an overlay method. Draw a set of equally spaced vertical lines on the cross section to represent the positions of columns to be restored. The spacing of the vertical lines controls the level of detail in the horizontal direction that will be obtained in the restoration. Draw a horizontal line on a transparent overlay to represent the restored datum. Mark the horizontal position along the datum line of each column to be restored. Shift the overlay to bring each column to the restored datum and mark on the overlay the position of each stratigraphic unit. Complete the restoration by connecting the stratigraphic horizons to form a continuous cross section.

If the cross section includes faults, their displacements can be removed in the restoration. In the simple shear model, fault displacement parallel to the regional is constant and equal to the hangingwall block displacement, ***D***. The steps in the restoration are given below (refer to Fig. 11.42 for the geometry).

1. Define the regional.
2. Find the block displacement by projecting a vertical line from the hangingwall cutoff of the reference bed to the regional. The block displacement is the distance ***D*** parallel to regional from the footwall cutoff of the marker bed.
3. Construct a series of vertical working lines, spaced ***D*** apart, starting at the fault.
4. To restore the hangingwall, each vertical segment along a working line in the hangingwall is moved up the fault until the horizontal component of displacement is equal to ***D***. The base of each segment remains in contact with the fault and the top marks the position of the restored reference bed. Record the position of each marker horizon along the working line.
5. Repeat step 4 for as many vertical hangingwall segments as necessary to produce a smooth restoration of the hangingwall beds.

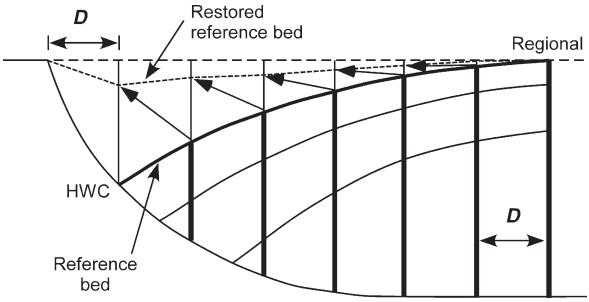

Fig. 11.42.
Restoration of a cross section by vertical simple shear above a fault. The net restoring displacement is parallel to the solid arrows. *D:* block displacement; *HWC:* hangingwall cutoff of reference bed

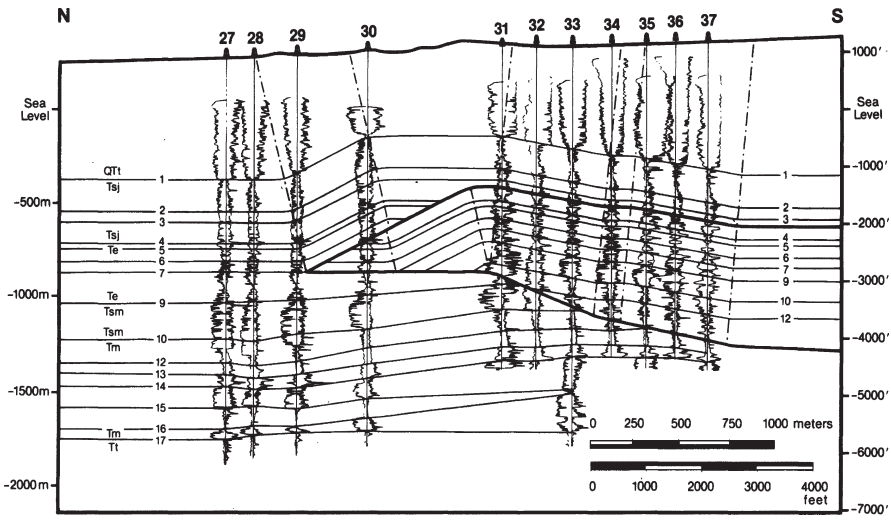

Fig. 11.43. Cross section of the thrust-cored Wheeler Ridge anticline, California (Medwedeff 1992). Wells show logs used for correlation of units

11.7.1.2 Pitfalls in Flattening

Restoration requires deciding whether a fold or fault is a pre-existing feature, to be passively deformed by the restoration, or is to control the restoration (an active feature). Fault-fold relationships are severely distorted if the hangingwalls of the active faults are not restored separately from the footwalls. As an example of the difference between restorations based on the active versus passive role of faults, consider the Wheeler Ridge anticline (Fig. 11.43). The cross section can be restored by treating the faults either as passive markers or as active elements with displacements that must be removed during restoration. Both alternatives are illustrated using the vertical simple shear technique. In both restorations the section is flattened to a datum at the top of the Tertiary San Joaquin Formation (Tsj). Assuming that the faults were passive markers, restoration (Fig. 11.44a) deforms the fault wedge but does not displace it horizon-

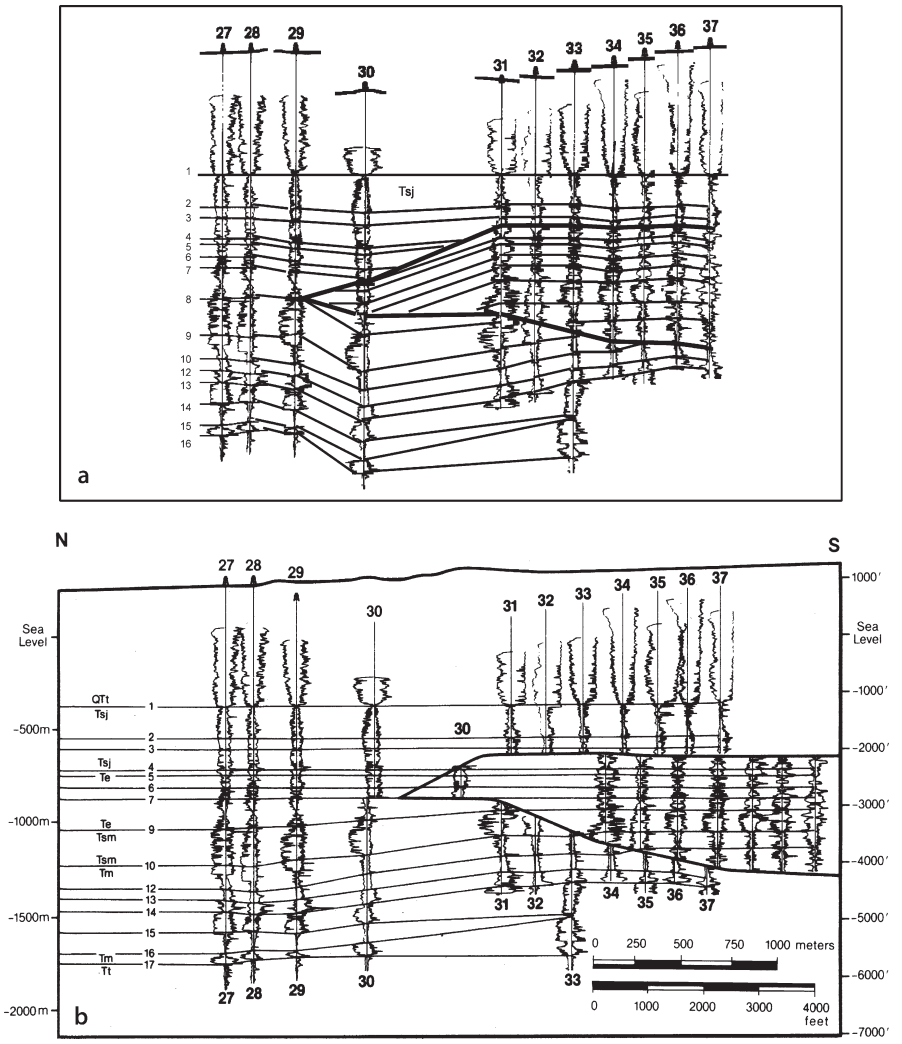

Fig. 11.44. Alternative restorations of Wheeler Ridge anticline (Fig. 11.43) by flattening to a datum at the top of the Tertiary San Joaquin Fm (Tsj, marker 1). Wells show logs used for correlation of units. **a** Flattening to a datum, disregarding possible slip on the faults. **b** Restoration by flattening to the Tsj datum with removal of fault slip (Medwedeff 1992)

tally. Assuming that the faults were active during the formation of the anticline, the fault wedge is restored by displacing the elements horizontally along the faults (Fig. 11.44b) so as to remove all of the hangingwall displacement. Which restoration is better is a geological decision. The restoration based on active faults (Fig. 11.44b) successfully flattens all the horizons down to horizon number 7, whereas the restoration based on passive faults (Fig. 11.44a) flattens only the original datum horizon. The

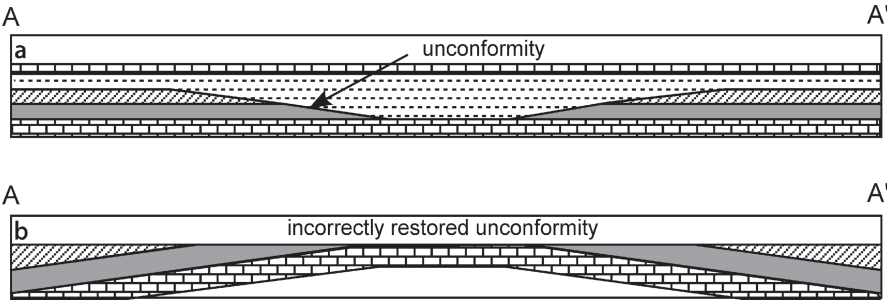

Fig. 11.45. Unconformity flattening pitfall. **a** Cross section of an undeformed unconformity and overlying valley fill. **b** Unconformity restored to horizontal showing an anticline that never existed

fault displacements in Fig. 11.44a must still be removed by a subsequent restoration. Based on the principles of simplicity and structural reasonableness, the restoration using active faults is a better representation of the geology at the time that the datum was horizontal.

Unconformities are not usually horizontal when they form, making the restoration of an unconformity a potential flattening pitfall (Calvert 1974). Flattening an unconformity to horizontal converts the original topography on an unconformity surface (Fig. 11.45a) into an anticline (Fig. 11.45b). The anticline indicated by the restoration was never present. An analogous problem occurs if the thickness variations of the unit directly above an unconformity are interpreted as representing a paleostructure when they, in fact, represent paleotopography. Interpretation of thickness variations in the shale overlying the unconformity in Fig. 11.45a as a paleostructure would lead to the interpretation of a growth syncline and the adjacent thinner areas as being growth anticlines, an incorrect interpretation of the true geometry in this example.

11.7.1.3 Oblique Simple Shear

The vertical simple shear concept can be generalized to shear in any direction (White et al. 1986). An oblique simple-shear restoration follows the same procedure as the vertical simple-shear restoration, except that the measurement lines are inclined to the regional at an angle other than 90°. The oblique lengths measured on the deformed-state cross section (Fig. 11.46a) are restored by translation in the shear direction to return the reference horizon to the regional (Fig. 11.46b). The spacing between any two measurement lines in the direction of the regional (S), and the shear angle (α), remains constant from the deformed state to the restored cross sections in both vertical and oblique simple-shear restorations.

The procedure for restoring a faulted section by oblique simple shear is analogous to the procedure for vertical simple shear except that the shear angle is less than 90°. The shear angle is measured downward from the regional. The fault displacement parallel to the regional is constant and equal to the hangingwall block displacement, ***D***.

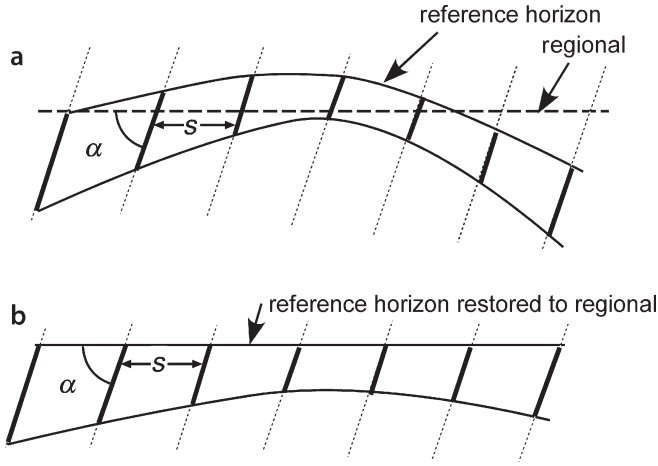

Fig. 11.46.
Restoration by oblique simple shear. *Medium-weight solid lines* are marker beds. *Dotted lines* represent the shear direction and are spaced an arbitrary distance *S* apart. The *widest lines* are the thicknesses in the shear direction to be restored. The shear angle is α. **a** Deformed-state cross section. **b** Restored cross section

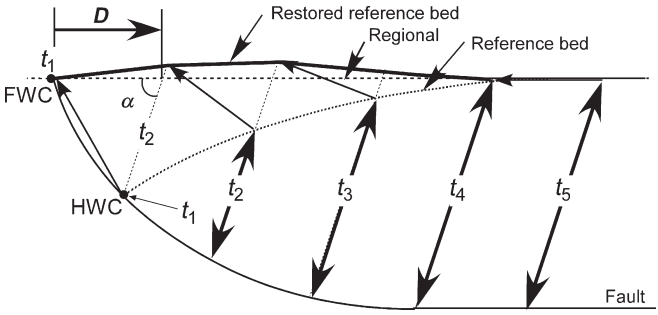

Fig. 11.47.
Restoration of the hangingwall of a fault by oblique simple shear. *FWC:* footwall cutoff of reference bed; *HWC:* hangingwall cutoff of reference bed; t_i: distance between reference bed and fault, measured along shear direction; α: shear angle; *D:* block displacement

Note that for oblique simple shear, ***D*** is not equal to the fault heave on the ramp, but is equal to the displacement on the lower detachment. The steps in the restoration are given below (refer to Fig. 11.47 for the geometry).

1. Find the regional.
2. The block displacement is found by projecting a line parallel to the shear angle from the hangingwall cutoff of the reference bed to the regional. The block displacement is the distance ***D*** from the footwall cutoff of the marker bed.
3. Along the regional, mark off equal distances, ***D***. Through each point draw a working line parallel to the shear direction, starting at the footwall cutoff of the reference bed.
4. Mark the position where each bed crosses a working line.
5. Each oblique segment of working line is moved up the fault a horizontal distance equal and opposite to ***D***. Keeping the base of the oblique segment in contact with the fault, mark the location of the top, which is the restored position of the reference bed. Mark the restored position of all the other beds along this restored oblique segment.
6. Repeat steps 4 and 5 until the hangingwall is restored.

11.7.2 Fault Shape Prediction Techniques

11.7.2.1 Vertical Simple Shear

The vertical simple-shear method for predicting the fault shape from the hangingwall geometry was developed by Roger Alexander of Chevron and used successfully for many years in the Chevron Oil Company (Verrall 1982). The technique is sometimes referred to as the Chevron or Verrall method. If the data are vertically exaggerated, the inferred bed or fault geometries will have the same vertical exaggeration as the data used, which may differ from that in the region into which projections are made.

To use vertical simple shear to predict fault shape from the hangingwall fold, three pieces of geological information are necessary: (1) the shape of the fold in a hangingwall reference bed, (2) the regional for the hangingwall reference horizon, (3) the block displacement in the direction of the regional (***D***). In order to correctly determine ***D***, the reference horizon must be correlated across the fault so that its hangingwall and footwall cutoffs are known. The technique is as follows (refer to Fig. 11.48 for the geometry):

1. Draw a straight line along the regional from footwall to hangingwall at the restored position of the reference bed.
2. Drop a perpendicular from the regional to the hangingwall cutoff of the reference bed.
3. Measure the fault separation parallel to the regional (***D***). Beginning at the footwall cutoff, mark equal distances along the regional with spacing equal to ***D***.
4. Drop perpendiculars from the regional at the equal-***D*** points to form working lines.
5. At a working line 1, measure the vertical distance from the regional to the fault.
6. Shift this measured length one ***D*** increment in the direction of transport (to line 2) and drop it down so that the top just touches the key bed in the rollover. The point marking the bottom of the vertical segment is the position of the fault.
7. Repeat steps 5 and 6, moving sequentially in the direction of transport (from line 2 to 11), until the section is complete.

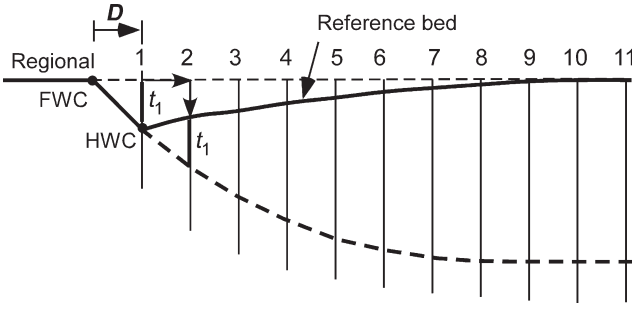

Fig. 11.48. Vertical simple-shear prediction of fault shape from rollover shape (after Verrall 1982). t_1 indicates the first vertical column that is shifted over ***D*** and down to the top of the reference bed. *FWC:* footwall cutoff of reference bed; *HWC:* hangingwall cutoff of reference bed; predicted fault is *heavy dashed line*

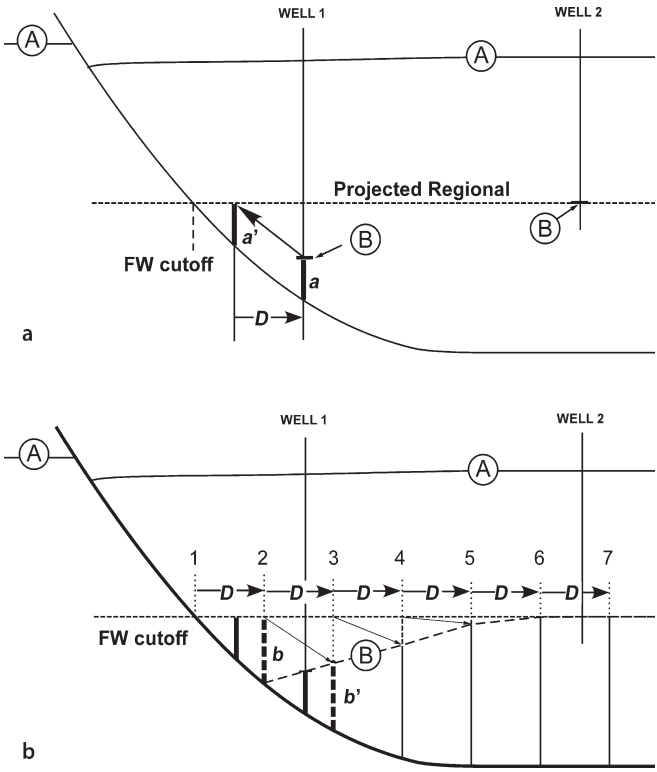

Fig. 11.49.
Determination of rollover shape from fault shape using vertical simple shear (modified from Verrall 1982). Marker A has been used to find the fault shape by the method of Fig. 11.48. The regional for bed B is obtained from well 2. **a** Determination of heave, ***D***. **b** Construction of position of marker horizon B; predicted shape is *dashed*

Once the shape of the fault is known, the geometry of any bed in the rollover can be determined if its regional position and the location of at least one point in the rollover is known (for example, B in Fig. 11.49a). The steps are as follows:

1. Find the regional by projecting a straight line along the regional from a known position of the regional in the hangingwall (B in well 2) to where it intersects the fault at the footwall cutoff. If the regional is known from the footwall, that level can be used for projection (Fig. 11.49a).
2. Drop a perpendicular from the regional, through point B in the rollover (in well 1) to the fault. The length ***a*** is the depth to the fault (Fig. 11.49a).
3. Move length ***a*** up the fault until it just touches the regional at ***a'*** (Fig. 11.49a).
4. The distance along the regional between ***a*** and ***a'***, is the heave (***D***) of marker B on the fault (Fig. 11.49a).
5. Starting from the footwall cutoff, mark equal distances along the regional at a spacing equal to ***D*** and draw perpendiculars to form the working lines 2–7 (Fig. 11.49b).
6. Measure the distance between the regional and the fault along working line 2 (***b***) and shift it one heave increment down the fault in the direction of displacement to line 3 (***b'***) where the top of the measured line marks the position of marker B (Fig. 11.49b).

7. Repeat step 6 for the remaining working lines to find the shape of marker B in the rollover (Fig. 11.49b).

In both the restoration and prediction techniques, the starting locations of the working lines are arbitrary. The requirement is that a unit thickness marked off along a working line is always shifted laterally one displacement increment (***D***). The original working lines may be spaced as closely as desired to retain the detail of the cross section. This is also true for the oblique simple shear technique, discussed next.

11.7.2.2 Oblique Simple Shear

The oblique simple-shear technique for predicting the fault geometry from the shape of a hangingwall fold is the same as the vertical simple-shear method but with oblique working lines. The construction steps are as follows (refer to Fig. 11.50 for the geometry).

1. Draw the regional.
2. From the hangingwall cutoff of the reference bed, draw a line parallel to the direction of simple shear (α from the horizontal) to its intersection with the regional.
3. The length ***D*** is the displacement of the hangingwall block necessary to produce the observed geometry. Mark off equal distances ***D*** along the regional, starting from the footwall cutoff.
4. At each displacement increment, draw a working line parallel to the shear direction from the regional to the vicinity where the fault is expected to be (lines 1–6).
5. Measure the length t_1. Shift this length in the displacement direction one ***D*** increment and move it down the shear line until the top of the line just touches the reference bed in the rollover (location t_1'). The bottom of the line segment is the location of the fault.
6. Repeat step 6 for the next line segment ($t_3 = t_1' + t_2$), and continue to repeat in the direction of displacement until the section is complete.

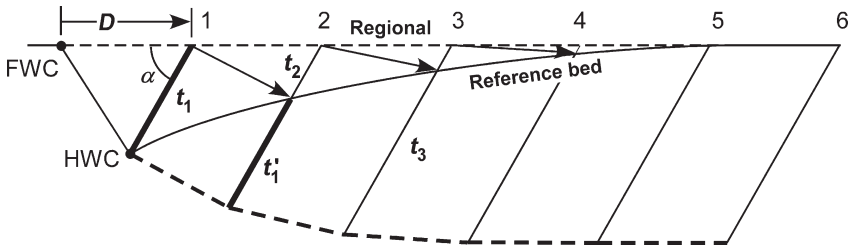

Fig. 11.50. Oblique simple-shear prediction of fault shape (*heavy dashed line*) from rollover shape. *D:* block displacement; *FWC:* footwall cutoff of reference bed; *HWC:* hangingwall cutoff of reference bed; predicted fault is *heavy dashed line*

11.7.3 Sensitivity of Prediction

For both vertical and oblique simple shear, the relationship between fault shape and the hangingwall rollover geometry is sensitive to (1) the shear angle, (2) fault dip between the hangingwall and footwall cutoffs of the reference horizon, (3) the stratigraphic correlation across the fault, and (4) the geometry of the reference bed near the fault (Withjack and Peterson 1993). Shape predictions are less sensitive to the exact location of the fault and to the rollover shape far from the fault.

Predictions are quite sensitive to small changes in the exact positions of the fault cutoffs. This is because small differences in the initial fault dip lead to errors that accumulate down the fault. From the opposite perspective, the agreement between observed and predicted fault trajectories is a sensitive indicator of the correct fault cutoff locations. Predictions are somewhat less sensitive to small changes in the correlation of the reference bed across the fault (Rowan and Kligfield 1989). Incorrect correlations also result in a mismatch between the predicted and observed fault trajectories. Additional discussions of simple-shear methods can be found in Wheeler 1987; Dula 1991; Withjack and Peterson 1993; Withjack et al. 1995; Hague and Gray 1996; Buddin et al. 1997; Shaw et al. 1997; Spang 1997; Hardy and McClay 1999; Novoa et al. 2000.

The major uncertainty in the simple-shear technique is in the choice of the shear angle. The next section describes the relationship between layer-parallel strain and the shear angle, followed by a discussion of how to choose the best shear angle.

11.7.4 Layer-Parallel Strain in Hangingwall

Simple shear oblique to bedding produces bed length and bed thickness changes (Sect. 11.3, Eqs. 11.14, 11.15) in beds above a fault. The relationships among the variables in Eq. 11.14 are illustrated by Fig. 11.51. For a normal fault, if the angle of simple shear is constant, the layer-parallel strain increases with the dip of the median surface of bedding, i.e., as a plane bed is rotated to steeper dips. Vertical simple shear produces much less strain for a given amount of bedding dip change than does oblique simple shear. Substantial dip changes without much strain imply vertical simple shear or that some other model is required. Synthetic simple shear (shear direction parallel to master fault) at angles lower than about 80° will cause layer-parallel contraction. Antithetic simple shear (shear direction dips opposite to master fault) produces layer-parallel extension. Small dip changes accompanied by readily visible second-order normal faults imply antithetic oblique simple shear, probably at angles of 60° or less.

The mechanism for the layer-parallel strain produced by oblique simple shear (Fig. 11.51) is usually small-scale faulting. The small-scale faults are probably not parallel to the shear direction, as logical as that may seem. The shear direction describes the geometry, not the mechanics. The faults produced by layer-parallel extension and the correlative thinning will be in response to the stress generated in the layer by the

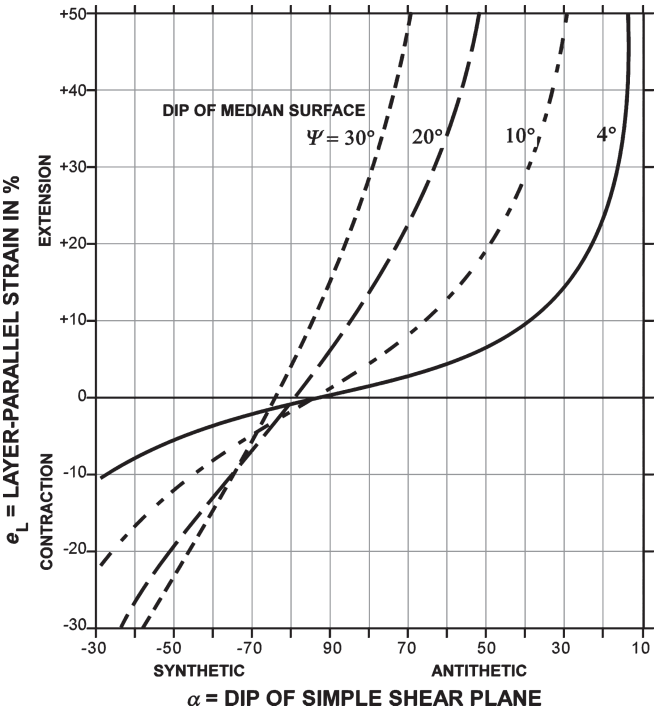

Fig. 11.51.
Layer-parallel strain in the hangingwall of a normal fault caused by simple shear oblique to bedding for various angles of dip of the median surface of bedding (Eq. 11.14, after Groshong 1990). All median surface dips shown are toward the master fault. Synthetic shear dips in the same direction as the master fault and antithetic shear dips opposite to the master fault dip

deformation. Thus conjugate faults or domino blocks are expected (Sect. 1.6.4) with orientations about 30° to σ_1. Because σ_1 is likely to be about normal to bedding, the expected faults should have initial dips close to 60°, regardless of the shear angle that connects the fault shape to the rollover geometry.

The structural styles that can be generated by small-scale faulting in a simple-shear rollover are illustrated with a series of forward models. Assume that the deformation mechanism in the rollover is the rotation of rigid dominoes with initial dips of 60°. The final geometry is controlled by the relative amounts and directions of (1) the external rotation of a median surface in the rollover, which is a function of the shear angle, and (2) the domino rotation, which is a function of the amount of layer-parallel extension (Sect. 11.5.2). The strain of the median surface is calculated from Eq. 11.14 and the domino rotation, given the layer-parallel strain, from Eq. 11.38.

Domino blocks bounded by faults that are precisely antithetic to the master fault at the beginning of deformation retain this geometry during extension (Fig. 11.52a). The domino-block rotation is exactly canceled by the rotation of the rollover. Dominoes that begin deformation with a steeper antithetic dip than the shear angle rotate away from the master fault during deformation (Fig. 11.52b). The net rotation of the domino blocks is relatively small. The geometries of Fig. 11.52a and 11.52b are common in the East African Rift valleys (Rosendahl 1987), the North Sea (Beach 1986), the Gulf of Suez (Colletta et al. 1988) and many other rifted environments. Dominoes that begin deformation dipping the same direction but at a lower angle than the shear angle rotate

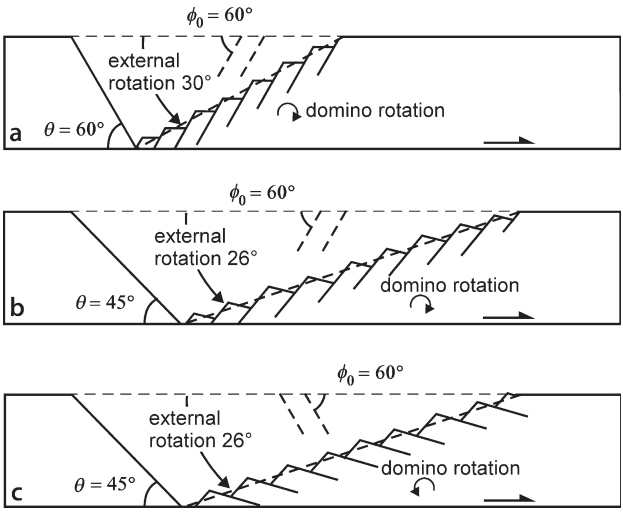

Fig. 11.52. Dominoes as the deformation mechanism in the rollover of a simple-shear half graben (modified from Groshong 1990). ϕ_0: initial dip of domino fault. The simple-shear direction in each rollover is exactly opposite to the dip of the master fault. **a** Dominoes begin with a dip exactly equal to the shear angle: domino rotation is equal and opposite to external rotation. **b** Dominoes begin with antithetic but steeper dip than the shear angle: domino rotation is opposite to and slightly greater than external rotation. **c** Dominoes begin synthetic to the master fault and with a steeper dip than the shear angle: domino rotation adds to the external rotation

a large amount toward the master fault because the external rotation and the domino rotation are in the same direction. The resulting low-angle normal fault geometry (Fig. 11.52c) is characteristic of the Basin and Range province of western North America. All the faults in the areas mentioned are not always parallel and the hangingwall extension may also be accommodated on conjugate normal faults.

11.7.5 Choosing the Best Shear Angle

It has been variously assumed that the shear angle is parallel to the dominant second-order fault trend (White et al. 1986), is exactly antithetic to the master fault (Groshong 1989), or is equal to the Coulomb failure angle of 30° to the maximum principal compressive stress direction (Xiao and Suppe 1992), but a variety of angles have been obtained in the laboratory and the field (Groshong 1990). The next sections examine methods for choosing the best angle.

11.7.5.1 Shear Angle by Trial and Error

One approach to finding the best shear angle is to find the angle that provides the best match between the shape of a bed in the rollover and the shape of the fault that

caused it (White et al. 1986; Rowan and Kligfield 1989). This approach, and its pitfalls, is illustrated by relating the rollover to the fault shape in two different versions of the same seismic section of a thin-skinned normal fault from the Texas Gulf of Mexico. In the first version (Fig. 11.53) the vertical scale is time and thus contains an uncompensated vertical exaggeration. The oblique simple shear method applied by

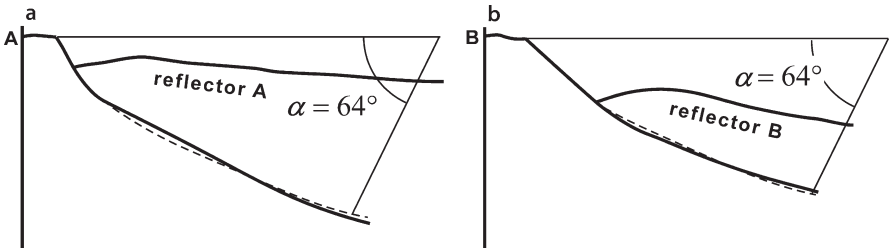

Fig. 11.53. Simple shear best fit to a normal-fault rollover on a seismic time section from Bruce (1973), modified from White et al. (1986). The *heavy solid lines* are drawn from the seismic line, the *dashed lines* are faults inferred from the model. **a** Best fit to reflector A, antithetic simple shear at 64° to the horizontal. **b** Best fit to reflector B, antithetic simple shear at 64° to the horizontal

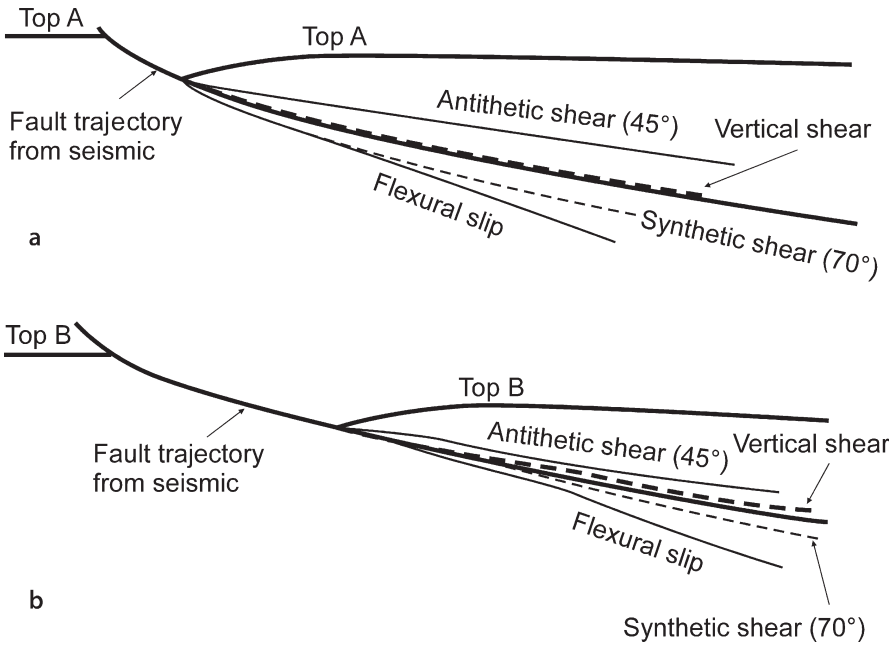

Fig. 11.54. Simple shear and flexural-slip best fits between rollover geometry and fault shape on depth-converted profile from Bruce (1973), redrawn from Rowan and Kligfield (1989). *Heavy solid lines* are from seismic line. **a** Marker A. **b** Marker B

White et al. (1986) gives a best-fit shear angle of 64° antithetic for two different reflectors on the same section (Fig. 11.53). Using a depth-migrated version (vertical exaggeration 1 : 1) of the same seismic line, Rowan and Kligfield (1989) predicted the rollover geometry using a variety of different shear angles (Fig. 11.54) and found that the angle that gives best match to the fault shape is 90° (vertical simple shear). This result demonstrates that an empirical best fit can be obtained in either time or depth but that finding the "true" shear angle requires a section without vertical exaggeration. The shear angle can compensate for an unknown vertical exaggeration but the strain related to the geometry and shear angle will only be correct if the shear angle is determined from an unexaggerated profile.

Additional confidence is obtained in the result if the same angle works for more than one bed as in both examples above. Statistical curve-fitting can be used to find the shear angle that minimizes the differences between the fault shapes predicted from multiple beds and to find the shear angle and shear azimuth in three dimensions (Kerr and White 1996).

11.7.5.2
Shear Angle from Axial Surface Orientation

The axial surfaces bounding dip domains in the pre-growth stratigraphy are parallel to the shear direction, a relationship that can be used to determine the shear angle (Fig. 11.55). Axial surfaces that are not parallel to the shear direction develop in growth sediments. See Xiao and Suppe (1992) and Spang and Dorobek (1998) for discussions of the geometry expressed by growth stratigraphy.

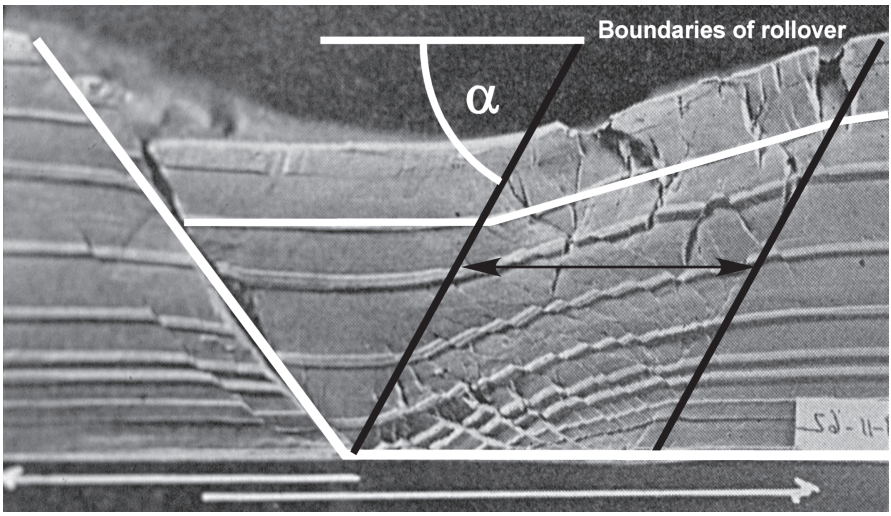

Fig. 11.55. Shear angle approximated as dip of axial surface (clay model from Cloos 1968, interpretation after Groshong 1990). The direction of oblique simple shear is given by the *heavy black lines*

11.7.5.3 Shear Angle from Strain

The layer-parallel strain is the basis of a third method to determine the best shear angle. The necessary relationship is derived by solving Eq. 11.14 for α (Groshong 1990). The result, Eq. 11.48, gives the appropriate shear angle from the layer-parallel strain and the dip of the median surface of bedding:

$$\alpha = \arctan\left[(e_L + 1)\ \sin\psi\right] / \left[(e_L + 1)\ \cos\psi - 1\right] \quad , \tag{11.48}$$

where α is the angle of shear measured from the regional, ψ is the angle of rotation of the median surface of the bed from the regional and e_L is the layer-parallel strain as a fraction. The layer-parallel strain will usually be seen as second-order faults in the rollover. From measurements of visible bed length and the total extent of the horizon, e_L is determined with Eq. 11.2.

This relationship has been tested on experimental sand and clay models by Groshong (1990), including the model in Fig. 11.55, and yields predicted faults that are a close match to the actual faults. The Livingstone Basin (Fig. 11.56a) provides a large-scale field example illustrating the shear-angle calculation. It is a sub-basin at

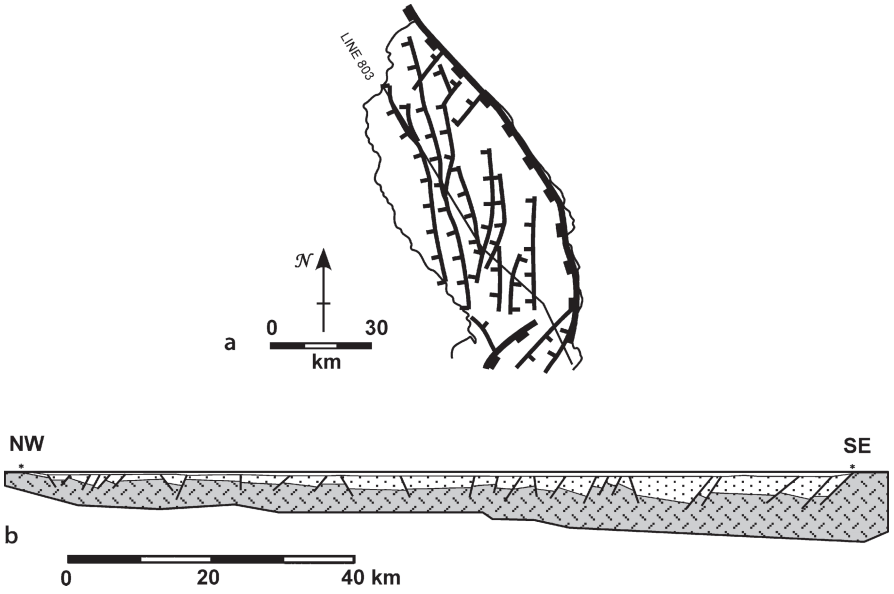

Fig. 11.56. Structure of Livingstone basin at the north end of Lake Malawi, East African Rift (after Wheeler and Rosendahl 1994). **a** Index map to Livingstone basin, showing the location of line 803. **b** Cross section along line 803, Livingstone basin, interpreted from depth-corrected seismic line (Wheeler and Rosendahl 1994). *Darker shaded unit* is basement, *lighter shaded unit* is sedimentary basin fill. No vertical exaggeration

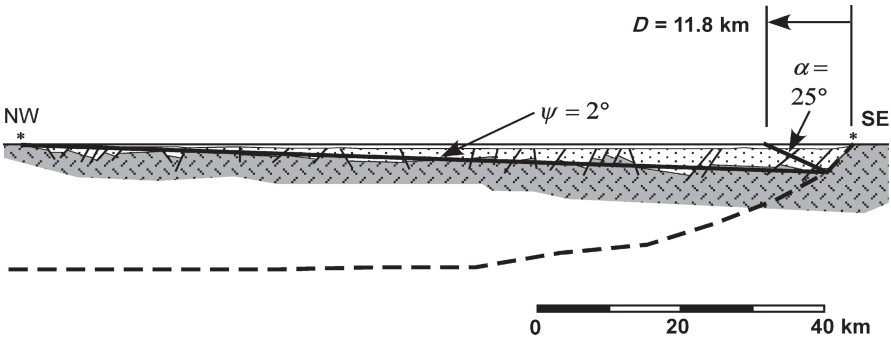

Fig. 11.57. Cross section in the transport direction of the Livingstone half graben (Fig. 11.56b), interpreted with the oblique simple shear model (Groshong 1995). *Darker shaded unit* is basement, *lighter shaded unit* is sedimentary basin fill. No vertical exaggeration. *Dashed line* is predicted fault

the north end of Lake Malawi (Nyasa), one of the East African Rift valleys. The master fault of the half graben is on the east side of the basin. The basin is broken by a number of second-order normal faults. The north-south trend of the faults within the basin seems to imply that the extension direction is east-west, however, the extension direction is interpreted to be northwest-southeast, oblique to the trend of the rift axis on the map (Scott et al. 1992; Wheeler and Rosendahl 1994). This interpretation is based on west-northwest to northwest plunging slickenlines on exposures of the master fault and on the presence of flower structures (wrench-fault indicators) along west-northwest trending faults in the basin. The cross section along the basin axis (Fig. 11.56b) is thus in the transport direction.

Using the relationship between layer-parallel extension and shear angle, it is possible to find the shape of the master fault, the depth to detachment, and the displacement that formed the graben. The amount of extension in the hangingwall is directly related to the dip change of the median surface and the angle of shear. Second-order normal faults are relatively evenly distributed throughout the hangingwall, as expected for the simple-shear model. The amount of extension along the median surface is determined by measuring the length of the top basement surface with and without the fault offsets and is $e_L = 0.08$ (Eq. 11.2). The dip of the median surface with respect to regional is $\psi = 2°$. From Eq. 11.48, $\alpha = 25°$. Given the shear angle, the shape of the master fault can be constructed by the oblique-shear method (Sect. 11.7.2.2) and is shown in Fig. 11.57. Measured from the figure, $H = 18.5$ km. By the oblique simple-shear model (e.g., Fig. 11.50), the displacement that formed the graben system is 11.8 km.

A depth of 18.5 km places the lower detachment of the Livingstone half graben in the middle of the crust. This depth is a reasonable possibility because it is the depth at which most seismic activity ceases below active cratonic rifts (Chen and Molnar 1983), even though the base of the crust is the expected location of the major strength minimum (Molnar 1988; Harry and Sawyer 1992) and rare deep earthquakes occur in the area (Shudofsky 1985; Jackson and Blenkinsop 1977).

11.8 Fault-Parallel Simple Shear

Fault-parallel displacement in the hangingwall is modeled with a slight modification of the vertical simple shear model (Williams and Vann 1987). The method uses a variable distance between working lines so as to maintain constant slip on the fault as it changes dip. This method approximates the hangingwall geometry developed above a listric normal fault in which there is nearly rigid rotation above the circular part of the fault, rigid-block displacement above the bedding-parallel fault segment, and a keystone graben between the rotated block and the translated block.

11.8.1 Restoration

The method for restoring a cross section by the constant dip separation model was developed by Chai (1994). The construction procedure is as follows (refer to Fig. 11.58 for the geometry):

1. Define the regional.
2. Draw a vertical working line through the hangingwall cutoff of the reference bed (point B).
3. Measure the straight-line dip separation on the fault, ***d*** (length AB).
4. Swing an arc from B of length ***d*** until it intersects the fault at C. This point locates the next vertical working line. Swing the next arc from C to find the location of D and so on. Draw vertical working lines through each marked point.
5. Measure the vertical distance from the reference bed to the fault, for example, t_1 the heavy line above point C, and shift it one working distance (W) horizontally and up the fault so that the base of the line is at the fault. The top of the line is the restored position of the reference bed. This is done for each vertical line to restore the section.

11.8.2 Fault-Shape Prediction

The construction of the fault geometry from the shape of a reference bed in the rollover is as follows (refer to Fig. 11.59 for geometry):

1. Define the regional.
2. Measure the straight-line dip separation, ***d***, along the fault between the hangingwall cutoff and the footwall cutoff of the reference bed.
3. Draw a vertical working line through the hangingwall cutoff of the reference bed. Swing an arc with radius ***d*** from point A at the intersection of the working line and the regional. Where the arc hits the reference bed marks the position of the next vertical working line, which defines point B.
4. Repeat the swinging of arcs of constant length equal ***d*** from the intersection of each vertical working line with regional to the reference bed until the rollover returns to regional.

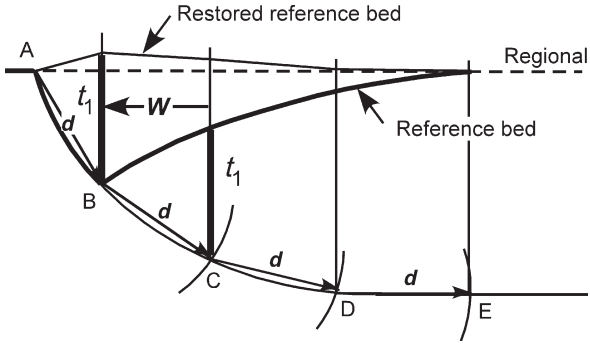

Fig. 11.58.
Restoration using the constant fault slip model (after Chai 1994). ***d:*** dip separation on fault; *W:* working distance between two working lines

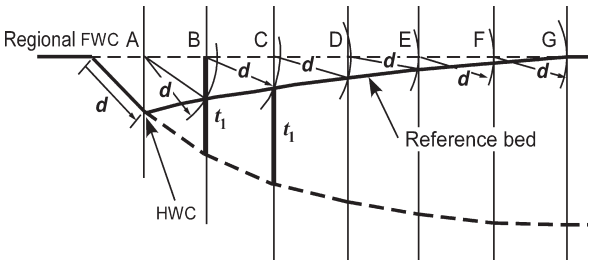

Fig. 11.59.
Fault shape prediction using the constant fault slip model (after Williams and Vann 1987). ***d:*** dip separation on fault; t_1: vertical distance between fault and regional below *B; HWC:* hangingwall cutoff; *FWC:* footwall cutoff; *thick dashed line:* predicted fault

5. Sequentially from the fault cutoff, shift the vertical thickness between the regional and the fault over one working distance in the direction of fault displacement, then move the thickness down the working line until the top just touches the key bed (for example, the thickness t_1 below B moves to below C). The position of the bottom of the line corresponds to the location of the fault. Repeat this step until the cross section is complete.

The constant fault slip model predicts the fault shape from the rollover geometry in a rigid-rotation experiment by Chai (1994). The hangingwall is homogeneous sand with layers of different colors, the fault is a pre-cut shape in a rigid block, and the extensional displacement is applied to the entire hangingwall by a flexible sheet on top of the footwall block, a configuration developed by McClay and Ellis (1987). The critical boundary condition in this experiment is that the flexible sheet forces the fault to maintain constant displacement and so the deformation mechanism is close to rigid rotation above the listric part of the fault. Characteristic of the model is the formation of a keystone graben between the rotated block above the listric portion of the master fault and the translated block above the lower detachment. The graben (Fig. 11.60) represents the strain required between the two differentially displaced nearly rigid blocks.

The constant fault slip model produces a better match between the rollover shape and the fault shape (Fig. 11.60) than any of the models described previously. The fit is close, although not exact. The lack of a perfect fit between the predicted and observed fault indicates that the best-fitting model does not perfectly duplicate the mechanics of deformation. Kinematic models are simplifications of the mechanical processes and so a close (but not necessarily perfect) match validates the interpretation.

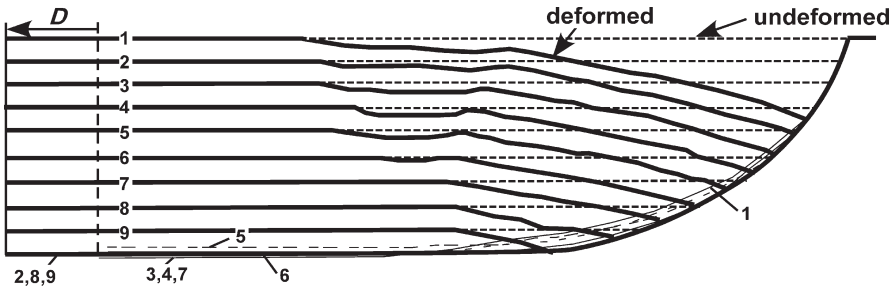

Fig. 11.60. Fault shapes predicted using the constant fault slip model for a sandbox experiment with constant fault displacement (Chai 1994). The predicted fault trajectories are numbered with the layer used to make the prediction. *D:* boundary displacement

11.9 Pure Shear Deformation

The final kinematic model to be discussed is pure shear deformation. The pure shear model is appropriate for the relatively uniform extension that forms a full graben. Significantly different predictions are produced depending on the dip of the boundary faults. The difference will be illustrated in a discussion of the Rhine graben.

11.9.1 Vertical-Sided Graben Model

Pure-shear extension of a vertical-sided graben (Fig. 11.61a) is the model proposed by McKenzie (1978) for the formation of an extensional basin. If this style of extension occurs above a rigid detachment (Fig. 11.61b), the subsidence of the graben is directly related to the amount of extension and the position of the detachment. If the extension occurs above a thick, deformable detachment unit (Fig. 11.61c), the amount of subsidence is controlled by isostacy and the temperature distribution (McKenzie 1978) in addition to the area balance of the graben. In this model the strain is uniform throughout the graben. The extension is usually calculated as the stretch, but based on the thinning, using Eq. 11.10.

11.9.2 Normal-Fault Bounded Graben Model

In this model the region of pure shear is bounded by normal faults and a planar detachment at the base (Fig. 11.62a). Extension causes the graben between the fault boundaries to stretch horizontally and thin vertically (Fig. 11.62b,c). The area-depth relationship provides a unique solution for the location of the lower detachment (Fig. 11.62d) and the strain is not uniformly distributed with depth.

The area-depth relationship, based on the deformed-state geometry of the 5 marker horizons in Fig. 11.62c, is a straight line (Fig. 11.62d) as expected for a locally balanced structure. The closeness of the area-depth points to the best-fit line through the data indicates the internal consistency of the cross section. The area-depth line goes to zero

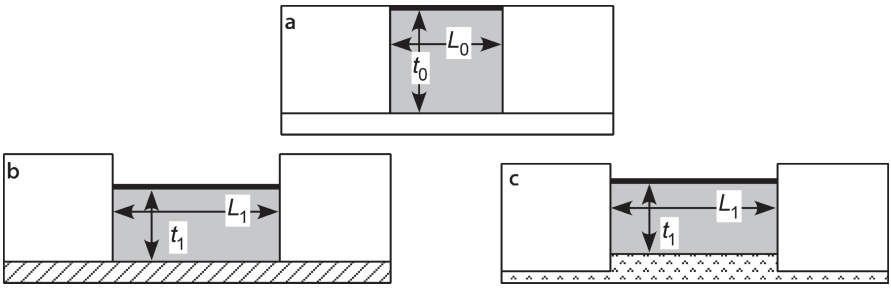

Fig. 11.61. Vertical-sided, area-balanced graben. **a** Before deformation. **b** After deformation, subsidence controlled by depth to the detachment. **c** After deformation, subsidence controlled by isostatic response of the system

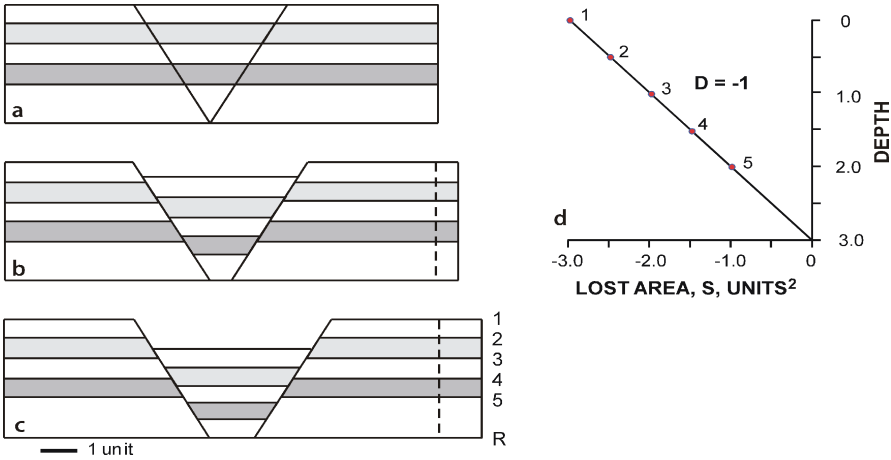

Fig. 11.62. Kinematic evolution of a pure shear full graben (after Groshong 1994). **a** Undeformed. **b** Initial stage of deformation. **c** Final stage of deformation. **d** Area-depth diagram of **c**. *Numbered points* correspond to *numbered horizons* in the cross section. Horizon 1 is the reference level

area at the lower detachment and the slope indicates a displacement of 1 unit. A model discussed previously (Fig. 11.18) is also a pure shear graben, but with growth sediments. Here the focus is on the internal strain in the graben.

Figure 11.63 shows the magnitudes of the layer-parallel strains for each horizon in the full graben model of Fig. 11.62c. The strain can be determined directly from the figure by comparing the bed lengths before and after the deformation (Eq. 11.2) as well as from the lost areas and depth to detachment as discussed in Sect. 11.4.3.2 (Eq. 11.26 or 11.27). Both methods give the same result. For this model the requisite strains are small in the upper part of the graben but increase rapidly toward the lower detachment and would approach infinity at the lower detachment because the original bed length there was zero. Quite a different strain magnitude is obtained if the total thickness change is used to calculate the extension (Eq. 11.10) as would be appropriate for a vertical-sided graben.

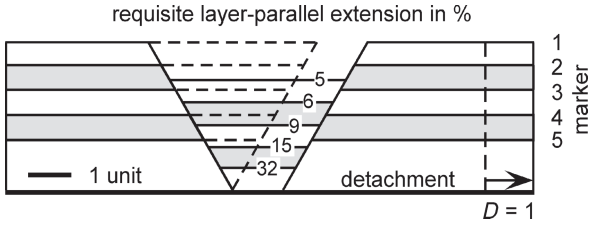

Fig. 11.63.
Strain in the graben of an area-balanced model (after Groshong 1994). The *dashed lines* indicate the position of the graben before deformation. Strain magnitudes are in percent

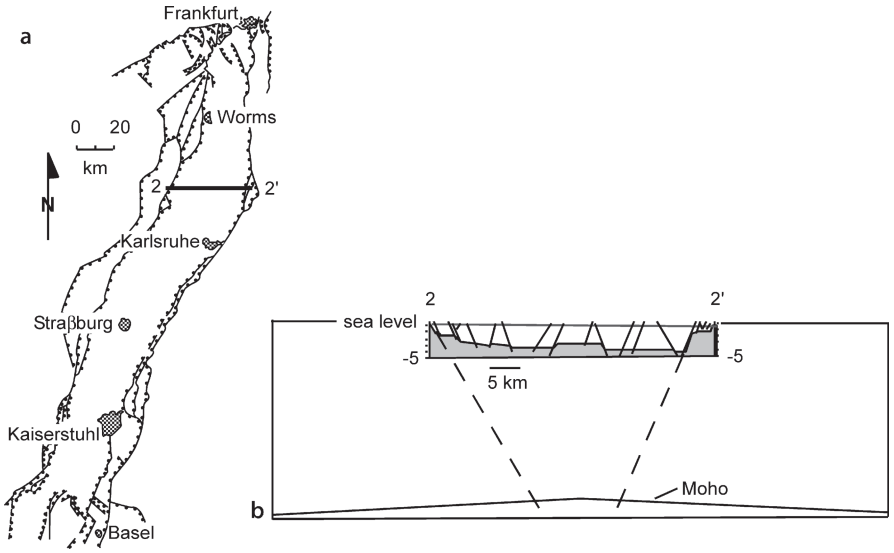

Fig. 11.64. Rhine Graben (after Groshong 1996). **a** Index map. **b** Cross section 2–2' inserted in a crustal profile. Triassic and younger sediments *unshaded*. The seismic refraction Moho is the base crust. (Illies 1977; Ziegler 1992; Rousset et al. 1993)

According to Eq. 11.11, the extension is $\beta_L = 1.34$ or $e_L = \beta_L - 1 = 34\%$ extension and is uniform with depth. This is clearly much different than the extension calculated directly from the model and shows the importance of the dip of the boundary faults.

The Rhine graben (Fig. 11.64a) provides an example of the dependence of the calculated extension on the model selected. The profile (Fig. 11.64b) is from the central area of the Rhine graben where it is relatively symmetrical, although the graben is asymmetrical to the north and south (Brun et al. 1992; Bois 1993; Rousset et al. 1993). The symmetry reverses across the profile area. The section to be interpreted was shown to be sequentially restorable by rigid block displacement in Fig. 11.9, thus it is valid. Length and area measurements were made on the preserved contact between the Permian and older basement and the Triassic Buntsandstein (shown in Fig. 11.9 and 11.64b).

Because shallowly buried rocks are both brittle and weak in extension, it is mechanically reasonable, although not certain, that nearly all of the layer-parallel extension within the sediments, including the Permian and older sediments of the shallow basement, occurs on the visible faults. The extension of the top-basement is 6.3% (Eq. 11.2), based on the bed

length of L_0 = 38.3 km, and the straight line distance across the top basement in the graben of L_1 = 40.7 km. The Moho is at a depth of 27 km directly below the graben and is 31 km deep outside it (Fig. 11.64b). The β value for the graben is 1.29 from Eq. 11.10 (e_L = 29%), assuming the original thickness of the crust in the Rhine graben was 31 km and the final thickness is 24 km (27 km minus 3 km of post-Permian sediments in the graben). The dramatic difference in extension calculated from the two different equations is the result of the specific pure-shear model applied. The large value is for a vertical-sided graben and the small value is the expected result near the top of a normal-fault-bounded graben. Because the Rhine graben has normal-fault boundaries, it is reasonable to conclude that the model of Fig. 11.63 applies to the graben and that the small strain magnitude at the top of the basement does not imply a major discrepancy in the extension, but rather is the expected value.

11.10 Exercises

11.10.1 Cross-Section Validation and Interpretation 1

Validate (or invalidate) the cross section in Fig. 11.65. Is it length balanced? Is it area balanced? Apply the area-depth relationship to find the best-fitting lower detachment, displacement, and the strain in each layer.

11.10.2 Cross-Section Validation and Interpretation 2

Validate (or invalidate) the cross section in Fig. 11.66. Is it length balanced? Is it area balanced? Apply the area-depth relationship to find the best-fitting lower detachment, displacement, and the strain in each layer.

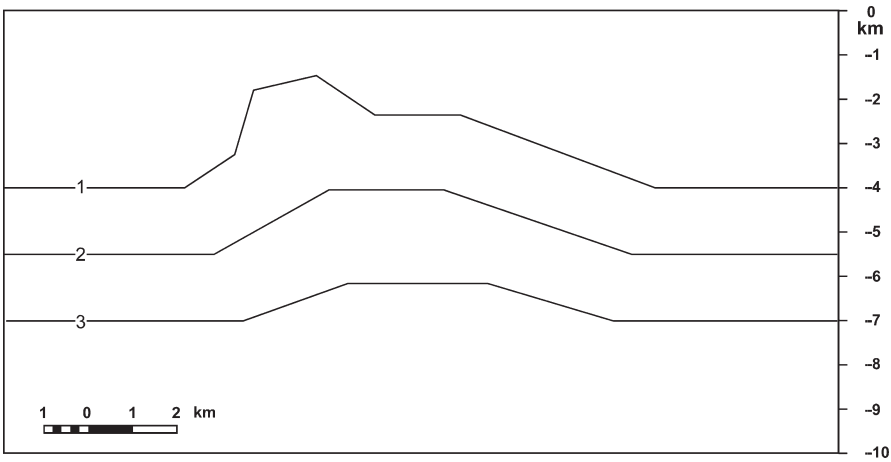

Fig. 11.65. Cross section of an anticline

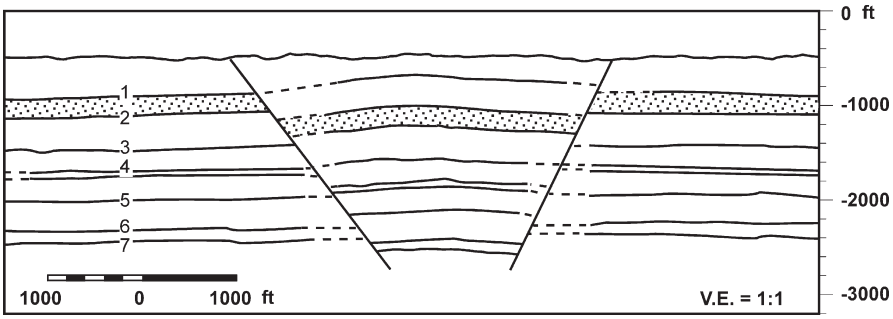

Fig. 11.66. Cross section of a full graben

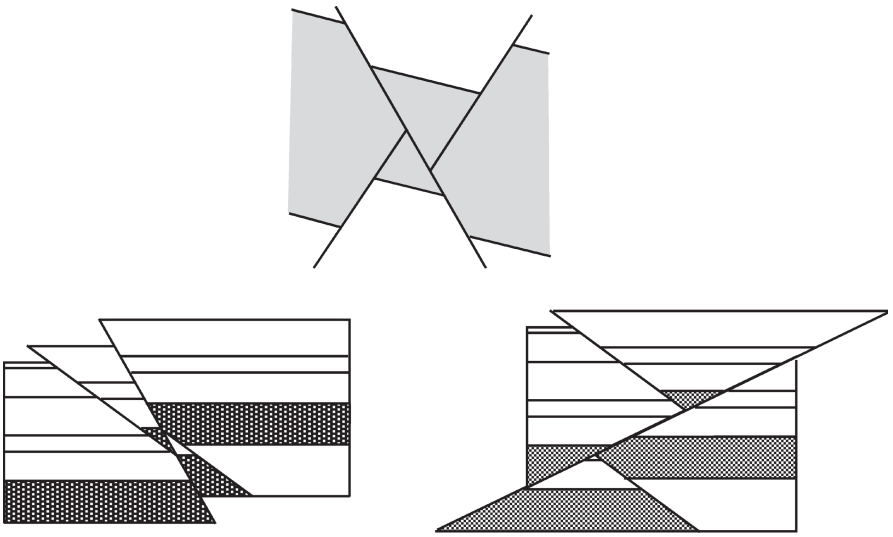

Fig. 11.67. Cross sections of structures formed by rigid-block displacement

11.10.3 Rigid-Body Restoration

Restore the cross sections in Fig. 11.67. Why is the rigid-body method appropriate? Are the cross sections valid? Show the structural evolution of each cross section.

11.10.4 Restoration of the Rhine Graben

Sequentially restore the cross section of the Rhine Graben in Fig. 11.68 to the top of the Bunte Niederroderner Schichten and the top of the Muschelkalk. What method is most appropriate? Is the cross section valid?

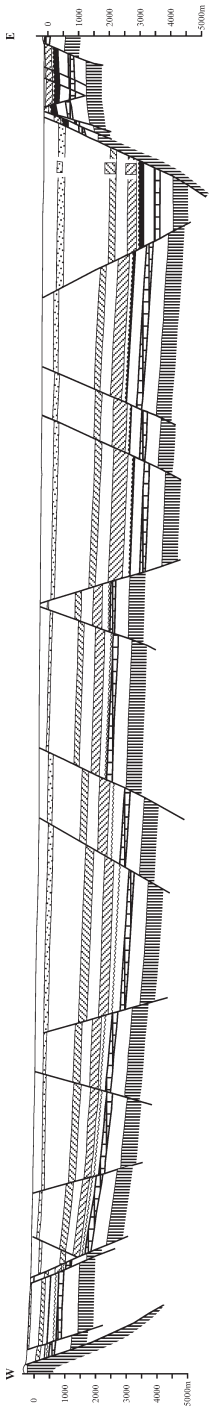

Fig. 11.68. Cross section of the Rhine Graben. (After Doebl and Teichmüller 1979)

11.10.5
Flexural-Slip Restoration 1

Restore the cross section of the Sequatchie anticline in Fig. 11.69. Why is the flexural-slip method appropriate? Discuss the effect of the choice of pin line and loose line on the result. Is the cross section valid?

11.10.6
Flexural-Slip Restoration 2

Restore the cross section of the Velma area in Fig. 11.70. Use the flexural slip technique and preserve the original stratigraphic thickness changes. Is the cross section valid? Discuss the origin of the major faults and their sequence of formation.

11.10.7
Flexural-Slip Restoration 3

Restore the cross section in Fig. 11.71 by flexural slip. First it is necessary to correlate units across the faults. Discuss the effect of the choice of pin line and loose line on the result. Could the interpretation be questioned or improved? Is the cross section valid?

11.10.8
Balance and Restoration

Restore the cross section of the Deer Park anticline (Fig. 11.72) by flexural slip or area balance, as appropriate. Construct an area-depth diagram for the entire anticline. What displacement caused the structure and what displacement is present on

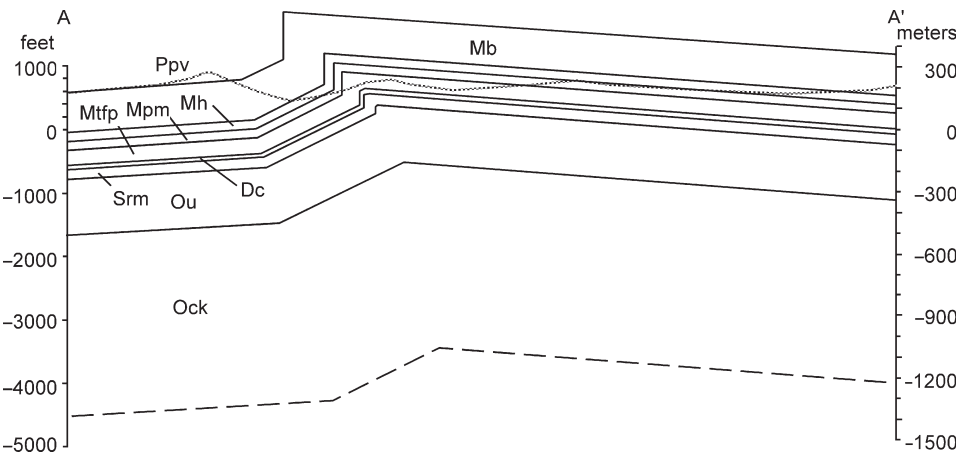

Fig. 11.69. Cross section of the Sequatchie anticline

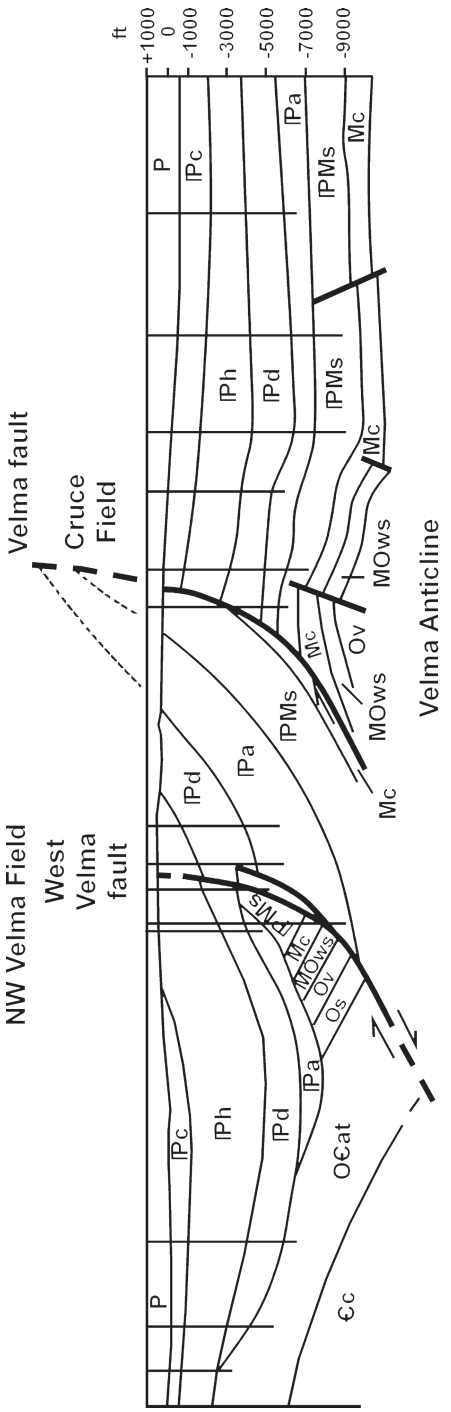

Fig. 11.70. Cross section through the Velma area, Oklahoma. (Redrawn from Perry 1989)

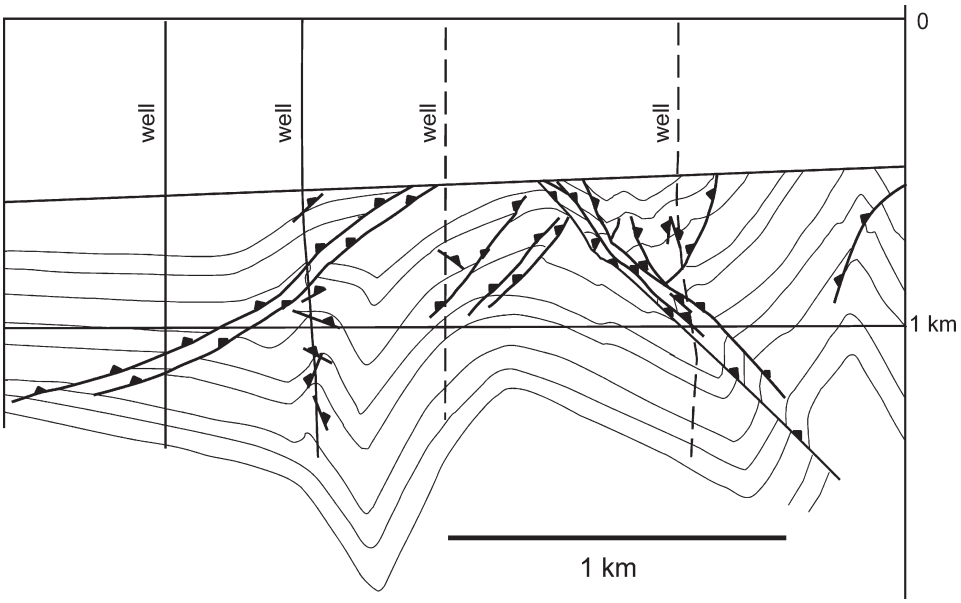

Fig. 11.71. Cross section of a portion of the Ruhr coal district, Germany. *Triangles* are located on the hangingwalls of the thrust faults. (After Drozdzewski 1983)

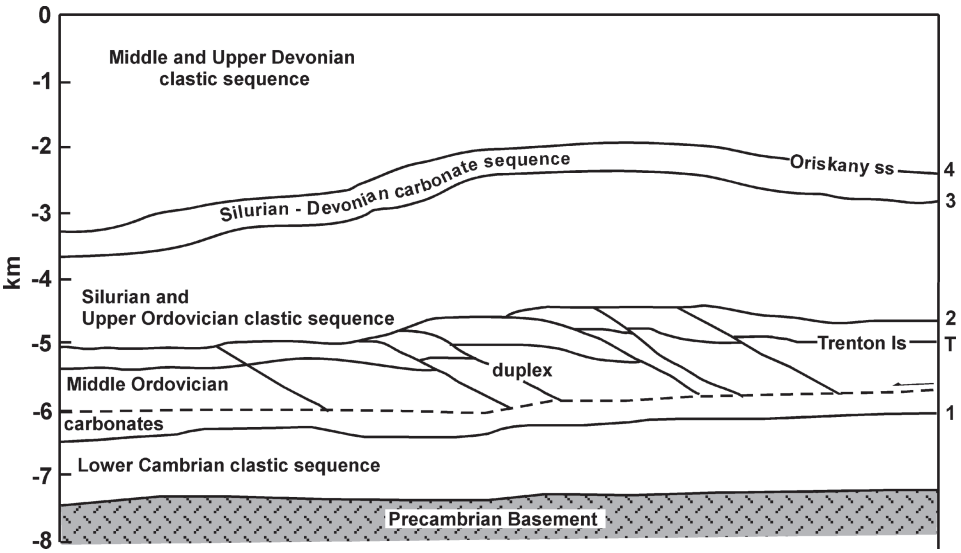

Fig. 11.72. Geological cross section across the Deer Park anticline, Appalachian Plateau fold-thrust belt, eastern U.S. The section is depth converted from Mitra (1986) using a velocity of 5 km s^{-1}. The inferred lower detachment is the *dotted line*. Epard and Groshong (1995) discuss the interpretation

the upper detachment, if any? Based on the results, is the structure locally balanced or regionally balanced? Compute the layer parallel strains for each layer. Is the cross section valid?

11.10.9
Predict Fault Geometry

The drape fold in horizons 1 and 2 in the South Hewett fault zone (Fig. 11.73) can be explained by an underlying rotated block. Apply the circular-arc fault model to predict the fault location and depth to detachment. The slip on some of the Zechstein normal faults has been reversed in the later deformation. Does the model explain which faults have reactivated?

11.10.10
Simple-Shear Restoration

Restore the growth normal fault in Fig. 11.74. This section contains growth stratigraphy and can be sequentially restored to the regional for horizons 2 and 3 to show the growth history. Why is the simple-shear method a reasonable choice? What is the appropriate choice of the regional? What is the most appropriate shear angle and how do you find it? Is the cross section valid?

11.10.11
Restoration and Prediction

Restore the cross section in Fig. 11.75 by either rigid-block displacement or flexural slip. Discuss the reason for your choice of method. Predict the deep geometry of the Schell Creek master fault using oblique simple shear. Find the shear angle from the strain in the rollover.

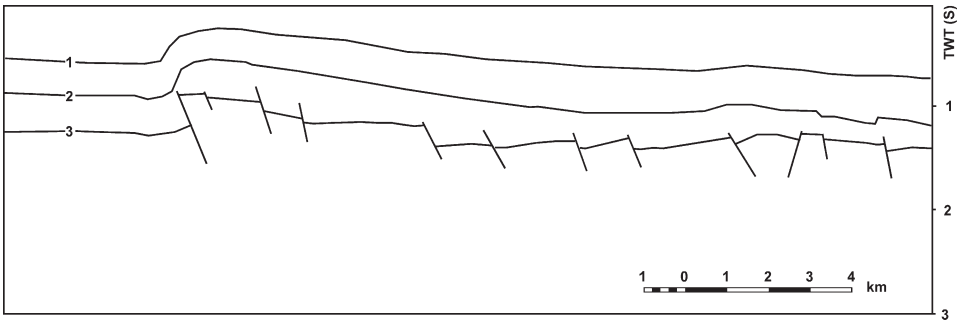

Fig. 11.73. The South Hewett fault zone in the North Sea. Interpreted and drawn from a seismic reflection profile in Badley et al. (1989). Assume the vertical exaggeration is approximately 1 : 1. Horizon *1:* top Cretaceous Chalk; *2:* base-Cretaceous unconformity; *3:* top Zechstein; *TWT(S):* two-way travel time in seconds

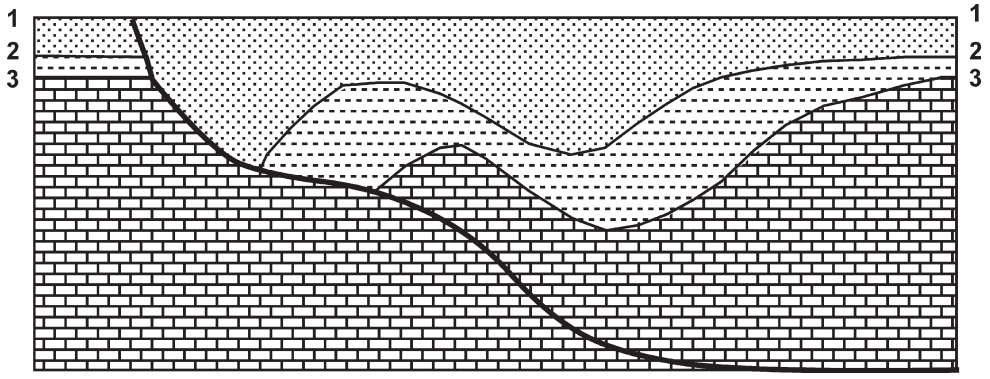

Fig. 11.74. Cross section of a ramp-flat normal fault

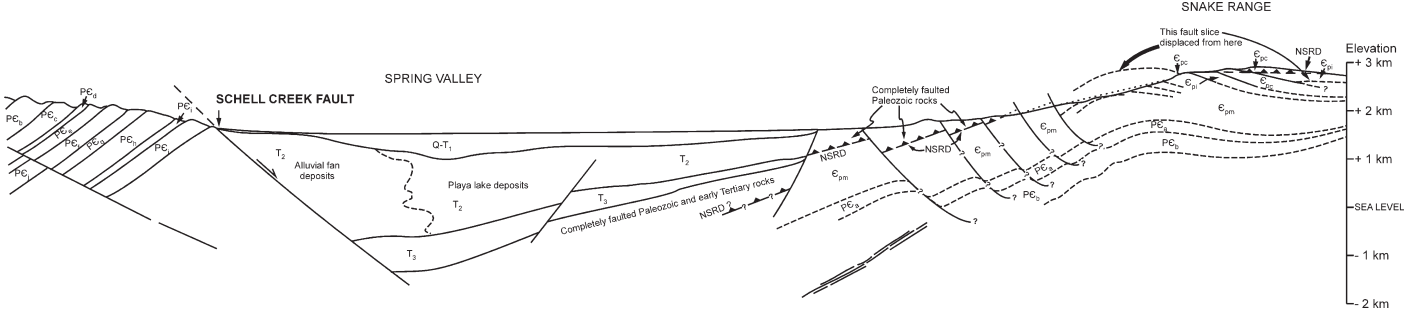

Fig. 11.75. Cross section of Schell Creek fault, U.S. Basin and Range province, Nevada from outcrop and seismic reflection profile. (After Gans et al. 1985). Groshong (1989) discusses the interpretation